



Numerical modeling of cosmogenic deglaciation records, Front Range and San Juan mountains, Colorado

Dylan J. Ward,¹ Robert S. Anderson,¹ Zackry S. Guido,¹ and Jason P. Briner²

Received 22 April 2008; revised 25 October 2008; accepted 24 December 2008; published 7 March 2009.

[1] We use cosmogenic radionuclide (CRN) exposure ages from polished, striated bedrock to constrain numerical simulations of deglaciation in the Middle Boulder Creek Valley, Colorado Front Range, and the Animas River Valley, San Juan Mountains, Colorado. In both valleys, the cosmogenic ages suggest initiation of deglaciation ~ 20 ka and ongoing retreat until 12–13 ka. While the first-order trend in CRN concentrations in each valley suggests a monotonic glacial retreat, we evaluate other retreat scenarios with different implications for post-Last Glacial Maximum regional climate. We use a 2-D numerical glacier simulation with a CRN layer to investigate how CRN-based deglaciation records are affected by retreat histories that are punctuated by periods of glacier readvance. The CRN layer simulates both production during periods of exposure and reduction by glacial erosion during readvances. We simulate glacial occupation of the valleys as they respond to equilibrium line altitude (ELA) histories characterized by stepwise change, gradual rise, or a rise punctuated by short periods of lowering. Each scenario generates a distinct spatial pattern of concentrations in the CRN layer. These results and the spatial pattern of measured concentrations in bedrock constrain the range of ELA histories that reproduce the CRN pattern in each valley. In the Animas River Valley, the exposure ages are well explained by a linear ELA rise from full glacial to deglacial conditions. Ages in Middle Boulder Creek Valley are best explained by a deglaciation history including a stillstand or partial readvance between 16 and 14 ka, followed by rapid retreat.

Citation: Ward, D. J., R. S. Anderson, Z. S. Guido, and J. P. Briner (2009), Numerical modeling of cosmogenic deglaciation records, Front Range and San Juan mountains, Colorado, *J. Geophys. Res.*, 114, F01026, doi:10.1029/2008JF001057.

1. Introduction

[2] Deglaciation records of alpine ice are valuable proxies for local and regional climate variability [e.g., *Oerlemans*, 1994; *Klok and Oerlemans*, 2004]. The complex dynamics of the climate-glacier coupling require that multiple lines of evidence constrain records of deglaciation. For example, ^{14}C ages in tarn sediment cores provide minimum limiting ages for headwater deglaciation [e.g., *Menounos and Reasoner*, 1997; *Toney and Anderson*, 2006], and ^{14}C and cosmogenic radionuclide (CRN) ages from glacial deposits constrain the timing of moraine stabilization following initial glacier retreat [*Benson et al.*, 2005; *Briner et al.*, 2005]. In situ ^{14}C , ^{10}Be , and other CRNs in bedrock can reveal the timing of deglaciation of specific sites on a glacier's bed, allowing retreat histories to be constructed in the absence of datable recessional moraines [e.g., *Nishiizumi et al.*, 1989; *Colgan et al.*, 2002; *Miller et al.*, 2006; *Guido et al.*, 2007]. Each of these methods has its own set of limitations and sources of

uncertainty, and in some cases, data sets are not directly comparable.

[3] Following the global Last Glacial Maximum (LGM; ~ 21 ka), alpine glaciers and ice caps throughout western North America (WNA) appear to have undergone a multi-phase retreat. Initial retreat from LGM positions occurred 18–21 ka in most dated localities [*Pierce*, 2003; *Kaufman et al.*, 2003]. After this initial retreat, another period of moraine formation is dated to between 15 and 17 ka; this probably represents a stillstand or readvance during deglaciation. In some locations, and particularly in the northern Rocky Mountains [*Licciardi et al.*, 2004; *Pierce*, 2003], this event appears to have overridden the LGM position. In more southerly or coastal locations such as the Sawatch Range [*Brugger*, 2005; *Briner*, 2007], and the Cascade Range and Sierra Nevada [*Kaufman et al.*, 2003], it is recorded as a second moraine set inside the LGM footprint. Rapid retreat appears to have been underway again by 14 ka across WNA and was largely complete by 12.5 ka. There is disagreement in the literature as to whether all of these phases were synchronous across WNA. Some have argued for broadly synchronous retreat across a wide range of latitudes [*Benson et al.*, 2005], while others argue for widespread variability in this timing because of spatial variations in available moisture [*Munroe et al.*, 2006], the influence of the Laurentide Ice Sheet [*Licciardi et al.*, 2004], and atmospheric transmission of North Atlantic

¹Department of Geological Sciences and Institute for Arctic and Alpine Research, University of Colorado, Boulder, Colorado, USA.

²Department of Geology, State University of New York at Buffalo, Buffalo, New York, USA.

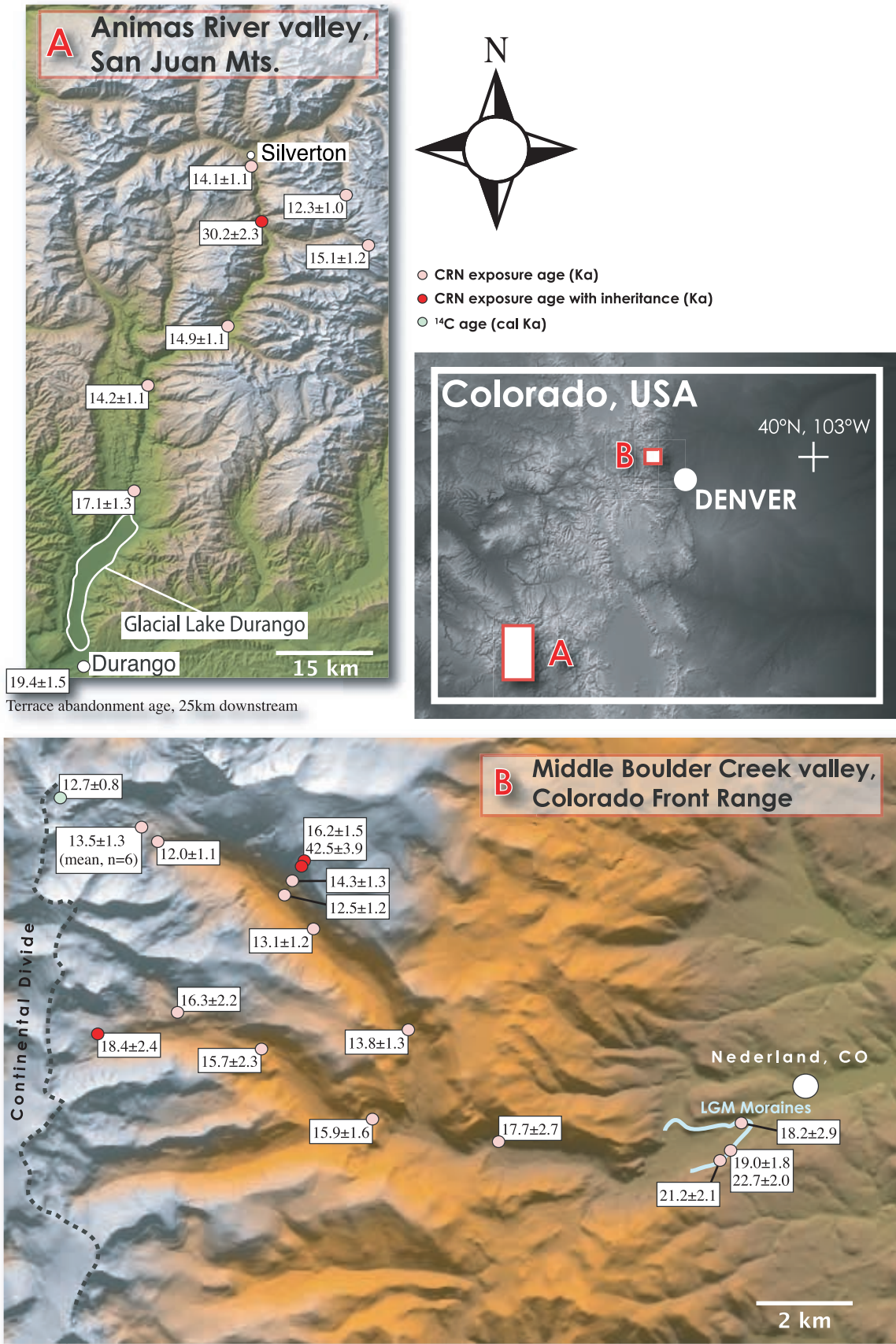


Figure 1

climate changes such as Heinrich events [Benson *et al.*, 1996; Hostetler and Bartlein, 1999; Hostetler *et al.*, 1999]. Responses of glaciers in WNA to millennial-scale fluctuations such as the Oldest Dryas cold period (following Heinrich H1; 17.5–14.7 ka) and the Younger Dryas (12.7–11.6 ka) cool period [e.g., Severinghaus and Brook, 1999; McManus *et al.*, 2004] are poorly constrained, with evidence from several locations supporting at least limited glacier growth in response to these events [Benson *et al.*, 1996; Gosse *et al.*, 1995a, 1995b; Menounos and Reasoner, 1997; Licciardi *et al.*, 2004].

[4] Records of the full deglaciation histories, and variations in retreat rate, of individual glaciers provide more insight into these problems than do ages that simply reveal the timing of initiation and completion of deglaciation. However, recessional moraines and sediments in glacial lakes are commonly absent, unrecognizable, or undatable. Cosmogenic exposure dating of glacially polished bedrock is an attractive alternative for constraining deglaciation histories, as datable surfaces are ubiquitous in many glacial valleys. Assuming that CRN inventory in a bedrock site is negligible prior to deglaciation of that site (see below), the exposure age should accurately record the time ice receded up valley and exposed the bedrock to cosmic rays [e.g., Nishiizumi *et al.*, 1989]. A suite of such ages in a profile along a deglaciated valley can be used to reconstruct the retreat history of the glacier's terminus [Guido *et al.*, 2007].

[5] Where such exposure histories can be meaningfully quantified, interpretation is not straightforward. In an ideal case, the CRN exposure ages record the position of the glacier's terminus throughout deglaciation. This position is related to climate through the hypsometry of the valley, so use of the retreat history to infer (for example) a history of equilibrium line altitude (ELA) during deglaciation requires at minimum that this hypsometric effect be taken into account.

[6] The CRN record of terminus retreat is itself an imperfect recorder of the retreat history. When all of the basic cosmogenic dating assumptions are met (e.g., no inheritance from exposure preglaciation, no erosion of a sampled surface since deglaciation, negligible or correctable bias by subsequent snow, sediment, and topographic shielding, appropriate CRN production rate scaling factors, and so forth), the exposure age versus valley distance trend will accurately record a *monotonic* retreat—one with no embedded readvances. Because deglaciation from the LGM is documented to have lasted many thousands of years across the western U.S. [Gosse *et al.*, 1995a, 1995b; Clark and Gillespie, 1997; Phillips *et al.*, 1997; Licciardi *et al.*, 2004; Guido *et al.*, 2007], while global and regional climate varied on much shorter timescales during that period [e.g., Benson *et al.*, 1998], we must acknowledge the reality that deglaciation histories are not monotonic but probably include short-term readvances during the protracted retreat. Such readvances impact the cosmogenic record of

deglaciation in the following two ways: (1) the distribution of exposure time during deglaciation at each point in a valley differs from that of a monotonic retreat and (2) erosion during readvances can strip some of the cosmogenic inventory accrued during the initial retreat, reducing the apparent exposure age.

[7] In this study, we use a 2-D numerical glacier simulation to explore the effects of valley hypsometry and non-monotonic deglaciation histories on CRN age records of deglaciation. We discuss these effects in the context of post-LGM glacier retreat histories in two deglaciated valleys in Colorado, USA, that we constructed using cosmogenic ^{10}Be exposure ages. We also present a method by which CRN samples with inheritance or anomalous shielding may be detected among a suite of samples that collectively describe a deglaciation history.

2. Cosmogenic Exposure Dating

2.1. Study Settings

[8] We use ^{10}Be exposure dating of glacially polished bedrock to constrain detailed post-LGM retreat histories for the Middle Boulder Creek Valley (MBCV), Colorado Front Range, and the Animas River Valley (ARV), San Juan Mountains, Colorado (Figure 1). In the ARV, a 90 km long outlet glacier of the LGM San Juan Mountain Icecap flowed south and terminated at the present location of Durango, CO. MBCV was occupied by an alpine glacier 20 km in length, beginning at the continental divide and terminating near the present town of Nederland, CO.

2.2. Sampling and Processing

[9] Our samples were chiseled from glacially polished bedrock to preclude corrections for erosion subsequent to deglaciation and on ice-sculpted knolls and sloped or wind-blown surfaces to minimize effects of snow and sediment shielding. Quartz was isolated and AMS targets prepared according to standard procedures at the University of Colorado Cosmogenic Isotope Lab; AMS analyses were performed by Lawrence Livermore National Laboratory and Purdue Rare Isotope Measurement Lab. Ages (Table 1) were determined from ^{10}Be concentrations using the CRONUS-Earth online calculator (<http://hess.ess.washington.edu/math/>, accessed 16 July 2008) [Balco *et al.*, 2008]. This assumes a sea level, high latitude (SLHL) production rate of 4.96 atoms $^{10}\text{Be}/\text{g}$ qtz/a by neutron spallation plus a small (~ 0.02 atoms/g/a) muogenic component, scaled to sample latitude and altitude using the routine of Stone [2000]. CRN ages used from the literature were rescaled as necessary to be directly comparable to our data.

[10] The errors we report on our ages are a combination of the 1σ analytical uncertainties and the stated $\sim 9\%$ error in the CRONUS production rate calibration (i.e., the “external error” reported by the calculator). The largest errors in our ages result from uncertainty in the appropriate

Figure 1. Locations of study sites, CRN sampling sites and resulting ages, and additional age constraints on deglaciation. Red outlying exposure age in the ARV was sampled from very hard quartzite and is interpreted to contain inheritance; in MBCV, outlying ages are from samples outside the glacial footprint (above the trimline), with the exception of the highest headwaters sample in the southern tributary. Ages in ka; errors include 1σ analytical uncertainty and production rate scaling uncertainty.

Table 1. Sample Names, Locations, and Age Results for Al and Be Samples, Using CRONUS-Earth Calculator v.2.1

Sample Name	Latitude (decimal degrees)	Longitude (decimal degrees)	Elevation (m)	Thickness ^a (cm)	Density (g/cm ³)	Shielding Correction	Erosion Rate (cm/a)	¹⁰ Be (10 ⁵ atoms/g)	¹⁰ Be ± ¹⁰ Be (10 ⁵ atoms/g)	²⁶ Al (10 ⁵ atoms/g)	± ²⁶ Al (10 ⁵ atoms/g)	Production Rate (atoms/g/a)	Exposure Age (years)	± Analytical (years)	± External (years)
<i>Middle Boulder Creek Valley</i>															
GP4J-1	40.0120	-105.6749	3549	3	2.7	0.991	0	7.529	0.237			55.85	13523	428	1251
GP4J-2	40.0111	-105.6741	3521	3	2.7	0.979	0	7.477	0.231			54.30	13813	427	1275
GP4J-3	40.0097	-105.6752	3520	10	2.7	0.995	0	7.045	0.256			52.09	13566	494	1279
GP4J-4	40.0088	-105.6742	3484	3	2.7	0.993	0	7.226	0.230			53.97	13433	430	1245
GP4J-5	40.0077	-105.6741	3463	2	2.7	0.988	0	7.052	0.227			53.74	13165	424	1221
GP4J-6	40.0103	-105.6681	3451	1	2.7	0.981	0	7.044	0.275			53.21	13280	519	1266
GP4J-7	40.0065	-105.6656	3434	1	2.7	0.986	0	6.352	0.201			53.01	12017	382	1112
GP4J-10	39.9713	-105.6043	2904	5	2.7	0.976	0	5.142	0.144			37.28	13840	390	1265
GP4J-11	39.9872	-105.6242	3051	5	2.7	0.972	0	5.282	0.191			40.53	13072	474	1232
GP4J-16	39.9550	-105.6112	2909	5	2.7	0.975	0	5.909	0.299			37.33	15891	807	1601
GP4J-20	39.9713	-105.6784	3436	4	2.7	0.992	0	9.739	0.912			51.97	18441	1734	2363
GP4J-21	39.9736	-105.6592	3301	2	2.7	0.993	0	8.193	0.849			49.05	16278	1693	2207
GP4J-22	39.9686	-105.6388	3106	7	2.7	0.990	0	7.016	0.797			41.90	15708	1791	2253
GP4J-23	39.9517	-105.5836	2708	5	2.7	0.979	0	6.131	0.758			33.28	17735	2201	2689
MB4J-0	39.9579	-105.5242	2590	5	2.7	1.000	0	6.112	0.817			31.45	18201	2442	2911
33-JB-25	39.9978	-105.6352	3162	3	2.7	0.978	0	5.528	0.181			44.26	12528	411	1164
33-JB-30	40.0017	-105.6337	3421	3	2.7	0.968	0	8.208	0.269			50.79	16221	534	1509
JB03-28	39.9995	-105.6319	3362	1	2.7	0.973	0	7.175	0.203			50.22	14336	407	1312
JB03-29	40.0022	-105.6334	3464	1	2.7	0.948	0	21.807	0.555			51.82	42493	1092	3877
99-474 ^b	39.9490	-105.5240	2646	1	2.7	1.000	0			43.226	2.066	206.31 (Al)	21170	1023	2118
<i>Animas River Valley^c</i>															
Baker's Bridge	107.79045	37.46771	2155	0.7	2.7	0.894	0	3.593	0.090			21.05	17067	551	1293
Tacoma	107.77917	37.56023	2285	2.5	2.7	0.917	0	3.301	0.116			23.23	14212	576	1131
Needleton	107.69437	37.62860	2540	0.6	2.7	0.918	0	4.153	0.104			27.91	14879	479	1126
Molas Lake	107.66169	37.73982	2828	0.5	2.7	0.925	0	10.180	0.243			33.76	30154	946	2279
Silverton	107.66853	37.78546	2835	3.5	2.7	0.482	0	2.429	0.064			17.25	14082	468	1072
Highland	107.58070	37.91239	3704	1.2	2.7	0.948	0	9.294	0.338			61.55	15100	510	1156
Mary Lake	107.54033	37.71465	3871	2.3	2.7	0.947	0	7.002	0.193			57.14	12254	515	982
Elk Creek	40.0000	-105.5580	2982	5	2.7	1.000	0	8.224	0.203	49.664	2.347	50.66	20644	512	1870
99-476 ^b	39.0700	-106.3030	2850	1	2.7	1.000	0	7.300	0.200	42.500	2.200	38.22	19184	811	1752
DC-91-2	39.0660	-106.3010	2810	1	2.7	1.000	0	7.000	0.300			37.30	18848	528	1831
DC-91-3															
<i>North Boulder Creek Valley</i>															
<i>Twin Lakes Valley, Sawatch Range^b</i>															

^aCRONUS calculator assumes 160 g/cm² attenuation scale for thickness corrections.

^bFrom Schildgen [2000].

^cFrom Guido et al. [2007].

Table 2. Middle Boulder Creek Valley and Animas River Valley Sample AMS Ratios and Background Data

Sample Name	Mass Clean Quartz (g)	Carrier Mass ^a (g)	AMS ¹⁰ Be/ ⁹ Be Ratio (raw)	AMS Ratio Error (1σ)	Background Correction (%)	AMS ¹⁰ Be/ ⁹ Be Ratio (corrected)	Corrected Ratio Error (1σ)	Ratio Error (%)
<i>Middle Boulder Creek Valley</i>								
GP4J-1 ^b	23.7357	0.3646	7.527E-13	1.786E-14	2.55	7.335E-13	1.789E-14	2.44
GP4J-2 ^b	19.9368	0.4108	5.623E-13	1.271E-14	3.42	5.431E-13	1.274E-14	2.35
GP4J-3 ^b	17.4205	0.4211	4.553E-13	1.320E-14	4.22	4.361E-13	1.323E-14	3.03
GP4J-4 ^b	18.3149	0.4188	4.921E-13	1.170E-14	3.90	4.729E-13	1.174E-14	2.48
GP4J-5 ^b	14.8832	0.4237	3.899E-13	9.277E-15	4.93	3.707E-13	9.323E-15	2.51
GP4J-6 ^b	9.4104	0.3993	2.676E-13	8.264E-15	7.18	2.484E-13	8.316E-15	3.35
GP4J-7 ^b	25.4258	0.4305	5.806E-13	1.376E-14	3.31	5.614E-13	1.379E-14	2.46
BLANK ^b	0.0000		1.921E-14	9.302E-16				4.84
GP4J-10 ^c	15.6580	0.3541	3.677E-13	1.032E-14	7.46	3.403E-13	1.032E-14	3.03
GP4J-11 ^c	11.6629	0.3531	2.885E-13	1.043E-14	9.50	2.611E-13	1.043E-14	3.99
GP4J-16 ^c	20.5953	0.3529	5.435E-13	2.750E-14	5.05	5.161E-13	2.750E-14	5.33
BLANK ^c	0.0000		2.742E-14	8.539E-15				31.14
GP4J-20 ^c	26.7354	0.3567	1.098E-12	4.301E-14	2.52	1.070E-12	4.301E-14	4.02
GP4J-21 ^c	21.9679	0.3565	7.611E-13	2.808E-14	3.63	7.335E-13	2.808E-14	3.83
GP4J-22 ^c	11.4350	0.3567	3.422E-13	1.846E-14	8.07	3.146E-13	1.846E-14	5.87
GP4J-23 ^c	20.8279	0.3567	5.413E-13	1.798E-14	5.10	5.137E-13	1.798E-14	3.50
MB4J-0 ^c	12.7756	0.3579	3.321E-13	2.769E-14	8.32	3.045E-13	2.769E-14	9.09
BLANK ^c	0.0000		2.762E-14	2.602E-15				9.42
33-JB-25 ^b	26.1411	0.3470				6.232E-13	1.614E-14	2.59
33-JB-30 ^b	17.9353	0.3358				6.561E-13	1.703E-14	2.60
JB03-28 ^b	16.2225	0.3561				4.891E-13	9.809E-15	2.01
JB03-29 ^b	23.6482	0.3535				2.183E-12	3.435E-14	1.57
<i>Animas River Valley</i>								
Baker's Bridge ^e	20.1760	0.3391	3.403E-13	7.922E-15	6.36	3.187E-13	8.012E-15	2.51
Tacoma ^e	22.8057	0.3438	3.481E-13	1.142E-14	6.19	3.266E-13	1.148E-14	3.52
Needleton ^e	17.9576	0.3449	3.441E-13	7.999E-15	6.27	3.225E-13	8.088E-15	2.51
Molas Lake ^e	15.1930	0.3427	6.881E-13	1.598E-14	2.49	6.709E-13	1.603E-14	2.39
Silverton ^e	20.0567	0.3444	2.340E-13	5.440E-15	9.83	2.110E-13	5.570E-15	2.64
Highland	13.0000	1.0094				1.346E-13	4.897E-15	3.64
Mary Lake ^e								
Elk Creek ^e	11.2582	0.9720				1.605E-13	4.415E-15	2.75
BLANK ^e	0.0000	0.35	2.536E-14	1.196E-15				4.72

^aThe concentration of Be in the carrier is 1000 ± 3 μg Be/g.

^bBackground corrections performed by Lawrence Livermore National Laboratory and include a <1% Boron correction.

^cBackground corrections performed by author (PRIME Laboratory) according to procedure outlined in CRONUS-Earth calculator documentation (http://hess.ess.washington.edu/math/docs/common/ams_data_reduction.pdf). No boron corrections.

Table 3. Middle Boulder Creek Valley and Animas River Valley Topographic Shielding Data^a

Sample Name	Azimuth (degrees)	Elevation (degrees)	Factor
<i>Middle Boulder Creek Valley</i>			
GP4J-1	0	14	0.991
	45	14	
	90	5	
	135	5	
	180	12	
	225	15	
	270	2	
GP4J-2	315	18	0.979
	0	29	
	45	19	
	90	-10	
	135	13	
	180	13	
	225	13	
GP4J-3	270	12	0.995
	315	19	
	0	9	
	45	7	
	90	4	
	135	12	
	180	10	
GP4J-4	225	14	0.993
	270	15	
	315	10	
	0	14	
	45	13	
	90	5	
	135	13	
GP4J-5	180	13	0.988
	225	9	
	270	16	
	315	13	
	0	11	
	45	15	
	90	5	
GP4J-6	135	19	0.981
	180	18	
	225	9	
	270	19	
	315	13	
	0	15	
	45	17	
GP4J-7	90	5	0.986
	135	5	
	180	20	
	225	15	
	270	21	
	315	24	
	0	14	
GP4J-10	45	15	0.976
	90	7	
	135	4	
	180	12	
	225	27	
	270	10	
	315	11	
GP4J-10	0	28	0.976
	45	24	
	90	10	
	135	5	
	180	15	
	225	19	
	270	19	
315	14		

Table 3. (continued)

Sample Name	Azimuth (degrees)	Elevation (degrees)	Factor	
GP4J-11	0	29	0.972	
	45	26		
	90	17		
	135	9		
	180	17		
	225	19		
	270	17		
GP4J-16 (from DEM)	315	12	0.975	
	GP4J-20	20		0.992
	50	15		
	80	12		
	115	15		
	155	10		
	195	20		
GP4J-21	215	10	0.993	
	240	6		
	260	2		
	285	0		
	300	5		
	15	16		
	95	9		
GP4J-22	110	14	0.990	
	125	12		
	150	13		
	205	18		
	320	2		
	355	10		
	65	16		
GP4J-23	135	14	0.979	
	160	22		
	290	6		
	310	0		
	345	5		
	360	12		
	10	15		
MB4J-0 (from DEM)	70	14	1.000	
	85	9		
	135	26		
	160	21		
	225	25		
	285	3		
	320	12		
33-JB-25 (from DEM)	<i>Animas River Valley</i>			
	Baker's Bridge	0	22	0.894
		45	27	
		90	31	
		135	19	
		180	6	
		225	29	
	270	38		
JB03-28 (from DEM)	315	44	0.973	
	0	5		
	45	21		
	90	38		
	135	21		
	180	14		
	225	20		
JB03-29 (from DEM)	270	26	0.968	
	315	44		
	0	5		
	45	21		
	90	38		
	135	21		
	180	14		
Tacoma	225	20	0.917	
	270	26		
	315	20		
	0	5		
	45	21		
	90	38		
	135	21		
180	14			
225	20			
270	26			
315	20			

Table 3. (continued)

Sample Name	Azimuth (degrees)	Elevation (degrees)	Factor	
Needleton	0	25	0.918	
	45	21		
	90	31		
	135	18		
	180	23		
	225	9		
	270	24		
Molas Lake	315	26	0.925	
	0	18		
	45	19		
	90	19		
	135	10		
	180	21		
	225	19		
Silverton	270	19	0.482	
	315	38		
	0	8		
	45	16		
	90	30		
	135	21		
	180	90		
Highland Mary Lake	225	90	0.948	
	270	90		
	315	90		
	0	1		
	45	2		
	90	15		
	135	17		
Elk Creek	180	12	0.947	
	225	16		
	270	10		
	315	10		
	0	2		
	45	15		
	90	5		
	135	4		
	180	20		
	225	9		
	270	2		
	315	2		

^aAll factors calculated using CRONUS-Earth Skyline code v.1.1. Shielding factors marked “(from DEM)” were taken from the model shielding factor grid as described in section 3.2, either because ground measurements were not obtained or were of poor azimuthal resolution.

scaling and time variability of cosmogenic production rates. The constant production rate model we used gives the oldest ages among the scaling routines reported by the CRONUS-Earth calculator; *Lifton et al.*'s [2005] scaling returns the youngest ages (7–12% younger), and the other time-dependent schemes [see *Balco et al.*, 2008] return ages between these end-members. As this error affects all of our samples approximately equally, and this paper is primarily concerned with interpreting the relative pattern of ages in a specific setting, these errors do not affect our fundamental conclusions but may influence the details of our climatic interpretations. As required by the version of the calculator we used (v. 2.1), our AMS ratio measurements were normalized with respect to the original ICN $^{10}\text{Be}/^9\text{Be}$ standard of *Nishiizumi et al.* [1984]. This standard assumes a ^{10}Be half-life of 1.5 Ma rather than the revised half-life of 1.37 Ma [Nishiizumi et al., 2007]. However, because our exposure ages are 2 orders of magnitude smaller than this half-life, they are little affected by this difference when used with the appropriately scaled production rate (as above). Tables 2 and 3 include the base data from which we calculated our samples' ages.

2.3. Resetting of Bedrock CRN Ages by Erosion

[11] Bedrock samples not completely reset by glacial erosion will contain CRNs from a prior period of exposure and will bias exposure ages to older values. Insufficient erosion most likely occurs where ice is thin, frozen to the bed, or sliding slowly (e.g., areas of low ice discharge) [Colgan et al., 2002]. Given the high rates of erosion by temperate glaciers [e.g., *Hallet et al.*, 1996], near-total resetting of the CRN inventory seems likely in the valleys studied here. For example, at a reasonable erosion rate of 1 mm/a, 3000 years of occupation lowers the bed by 3 m and reduces the CRN concentration to <1% of its initial value.

[12] In both the ARV and MBCV, several lines of evidence suggest that inheritance can be ignored for the purposes of this study. In the ARV, ^{10}Be inheritance measured in a river terrace derived from sediments eroded by the Animas glacier is effectively zero, implying enough erosion by the glacier to reset the CRN inventory of the valley floor, on average [Guido et al., 2007]. In both valleys, ^{10}Be ages generally decrease up valley (within error), and all ages fall between bracketing ages of initial retreat (moraine boulders in MBCV and terrace abandonment age in the ARV) and cirque deglaciation as documented by calibrated ^{14}C ages from basal sediments of tarns. The sole exception is a sample in the Animas Valley that was collected from a quartzite knoll whose hardness likely minimized erosion. For the purposes of this study, we therefore assume zero initial concentration of ^{10}Be in the bedrock upon exposure by deglaciation.

[13] We investigate the potential that this assumption misleads us by calculating the range of erosion depths at which inheritance is “problematic.” That is, at some depth of erosion, the inherited signal is reset to within analytical error on a ^{10}Be concentration measurement, as we have assumed is the case throughout this study. Erosion that is shallower than a particular depth will leave enough inheritance that the apparent exposure age will be “out of bounds,” i.e., older than the LGM moraine. Erosion values between these extremes will leave an amount of inheritance that will impact the exposure age, but not to the extent that it is obviously out of bounds. For the dominant spallation mechanism, we can solve for the thickness of this zone of problematic inheritance as a function of the “true” exposure age at a sample location (which we strive to determine).

[14] Starting with the top of this zone, we wish to find the line below which the inherited concentration (C_{inh}) is lower than the concentration (C_{max}) corresponding to the difference between the bounding age of the LGM moraine (T_{max}) and that corresponding to the true exposure age at the site (C_e , T_e)

$$C_{\text{inh}} \leq C_{\text{max}} - C_e. \quad (1)$$

The concentration at a given depth reflects the product of the time of exposure with the production rate at that depth, which for neutron spallation falls off exponentially with increasing depth. Using this relationship, we can introduce depth z

$$P_0 T_{\text{inh}} e^{-\frac{z}{\lambda}} = P_0 T_{\text{max}} - P_0 T_e, \quad (2)$$

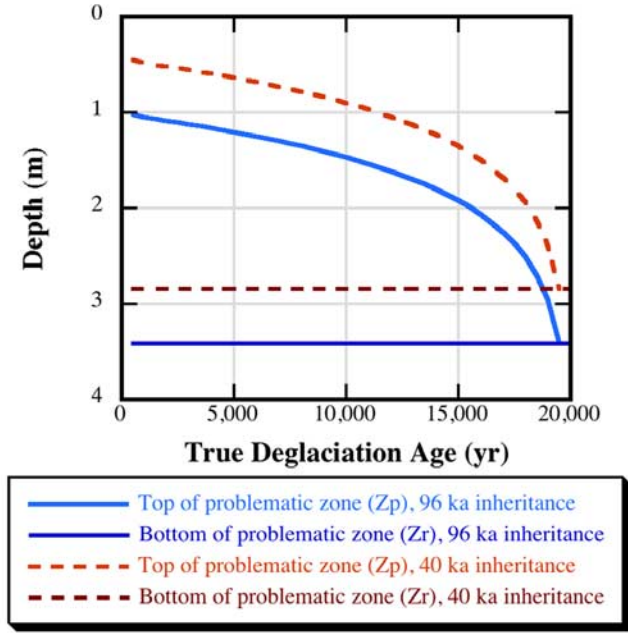


Figure 2. Depth range of erosion where an amount of inheritance remains sufficient to bias an exposure age without rendering it out of bounds. The position of the top of this zone (Z_p) is set by the difference between the bounding age and the true exposure time at the site; the bottom (Z_r) is defined as the depth of erosion needed to reset the CRN inventory to within analytical error. Here, $z_* = 0.65$ m for ^{10}Be production in granitic rock, and the bounding age is assumed to be a terminal moraine independently dated at 20 ka. Note that the thickness of the zone does not depend on the initial inherited concentration but the absolute depth of it does.

where z_* is the e -folding length scale for decline of production with depth, and P_0 is the surface production rate at the sample site. We can now solve for the depth z_p to which erosion must proceed to leave an inherited signal that is sufficient to be problematic

$$z_p = -z_* \ln \left[\frac{T_{\max} - T_e}{T_{\text{inh}}} \right]. \quad (3)$$

[15] The bottom of the zone of problematic inheritance, z_r , is simply where $C_{\text{inh}} \leq C_{\text{err}}$, where C_{err} is the analytical error limit for cosmogenic nuclide concentration measurement

$$P_0 T_{\text{inh}} e^{-\frac{z_r}{z_*}} = P_0 T_{\text{err}}, \quad (4)$$

where T_{err} is the surface exposure time needed to produce concentration C_{err} . Solving for the depth as before

$$z_r = -z_* \ln \left[\frac{T_{\text{err}}}{T_{\text{inh}}} \right]. \quad (5)$$

We plot these curves in Figure 2. Note that the closer the true exposure age to the bounding maximum age, the

smaller the zone in which a problematic inherited signal will remain. For a given true exposure age, bounding age, and z_* , the thickness of the problematic zone is constant regardless of the initial inheritance, but its absolute depth scales with the initial inherited concentration. Given the ~ 2.5 m thickness of this zone, a fairly large range of erosion depths will cause problems in our age estimates. However, the up-valley-decreasing trend seen in our age patterns would seem to require an extraordinary coincidence of erosion rate pattern to be caused solely by problematic inheritance. Below, we discuss a method by which individual data points with problematic inheritance may be detected.

2.4. Cosmogenic Exposure Dating Results

[16] Our cosmogenic sample locations, scaling corrections, and other detailed information can be found in Table 1. Exposure age-distance profiles for the ARV and the MBCV main tributary can be characterized as monotonic with some scatter, with ages generally decreasing up valley (Figure 3). Exposure ages in the MBCV south tributary are consistently higher than those in the main valley, but none of these are older than the terminal moraine. Neither ARV nor MBCV has obvious recessional or readvance deposits within the LGM glacial footprint, except for some small hummocky deposits in the south tributary of MBCV.

[17] We calculate an exposure age for the terminal moraine on the basis of several cosmogenic data sets, all rescaled to equivalence with the cosmogenic production schemes used for our own data. In rescaling ^{36}Cl ages, which reflect a different production mechanism than do ^{26}Al and ^{10}Be ages, we conservatively double the reported error ranges to reflect our ignorance of the conversion from Cl to Be years. The resulting error ranges are about the same size as those on the Al and Be data. Our data set consists of one ^{10}Be boulder age from this study (18.2 ± 2.9 ka), two ^{36}Cl ages from boulders on this moraine from *Benson et al.* [2005] (19.0 ± 1.8 and 22.7 ± 2.0 ka), one ^{26}Al boulder age from *Schildgen* [2000] (21.2 ± 2.1 ka) and one ^{10}Be boulder age from the terminal Pinedale moraine in N. Boulder Creek Valley, ~ 5 km north of MBCV (20.6 ± 1.9 ka). We calculate the error-weighted mean of these data by assuming normally distributed errors on each age, then weighting each by the inverse of its variance ($1/\sigma^2$). The reduced χ^2 of this data set is 0.6, and the weighted mean is 20.0 ka (Figure 4). The weighted and arithmetic means differ by merely 30 years. The biased weighted standard deviation is 1.4 ka; because of the small size of our data set, we prefer the unbiased estimated population standard deviation of 1.5 ka. We thus assign an age of 20.0 ± 1.5 ka (1σ) to the terminal moraine. Excluding the less reliable ^{36}Cl ages from the data set reduces this age by 300 years, or 1.5%.

[18] We present 18 new cosmogenic exposure ages from glacially polished bedrock sampled in the Middle Boulder Creek Valley. All of these ages are younger than the terminal moraine boulder ages. Ages appear to decrease monotonically with distance up valley from the moraine, and the several ages in the uppermost headwaters are uniformly ~ 13 ka. This closely agrees with a radiocarbon age of 12.0–13.5 cal ka (2σ) from basal sediments in Lake Dorothy, a tarn in one of the cirques of MBCV [*Davis et al.*, 1992] calibrated using CALIB v. 5.0.1 [*Stuiver and Reimer*,

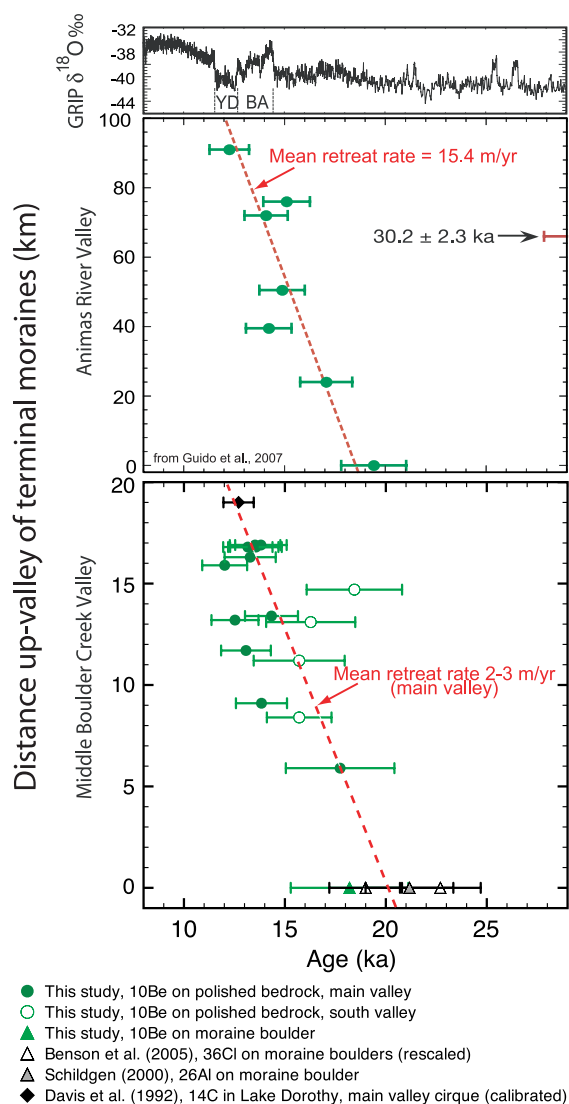


Figure 3. Exposure age versus distance up valley for the (top) ARV and (bottom) MBCV. Both retreat histories can be expressed as monotonic, with some scatter. In both valleys, retreat begins and ends at roughly the same time, but the greater length of the Animas glacier dictates a faster mean retreat rate. Greenland Ice Core Project (GRIP) $\delta^{18}\text{O}$ record is shown for reference (Figure 3 (top)). YD is the Younger Dryas cool period, and BA is the Bølling-Allerød warm period. Both records hint at faster retreat beginning ~ 14 ka. Error bars on ages include 1σ analytical uncertainty and production rate scaling uncertainty.

1993] with the calibration data set of Reimer *et al.* [2004]. Four of our ^{10}Be ages lie in a cross section across the midvalley, which reveal a pattern of post-LGM ages (12–14 ka) within the glacial footprint, and older, unreset exposure ages (~ 40 ka) above the trimline.

[19] Interpreting the terminal moraine age as dating the initiation of retreat, the mean rate of retreat of the MBCV glacier was ~ 2.5 m/a, and began promptly after the global LGM (~ 21 ka). Deglaciation was complete by the onset of Younger Dryas time, ~ 13 ka.

[20] Data from the Animas River Valley show a similar age trend. Deglaciation began at 19.4 ± 1.5 ka, on the basis

of a ^{10}Be depth profile in a Pinedale age proglacial river terrace [Guido *et al.*, 2007]. A longitudinal transect of exposure ages on glacially polished bedrock indicates that terminus retreat was relatively steady at ~ 15 m/a until complete deglaciation around 12.3 ka, although the data allow for an increased rate of retreat ~ 15 –13 ka. Deglaciation time of individual cirques varies and is apparently dependent on topographic aspect. As in MBCV, the cosmogenic ages agree well with calibrated radiocarbon ages from bogs and lakes within the glacial footprint [Andrews *et al.*, 1975; Elias *et al.*, 1991; Toney and Anderson, 2006]. For a more detailed discussion of the deglaciation of the ARV, refer to Guido *et al.* [2007].

[21] Within error, the timing of initiation and completion of deglaciation was similar in both MBCV and ARV. These dates agree well with many other records from western North America, wherein deglaciation begins at or shortly after global LGM, and is generally complete by early Younger Dryas time, with evidence only supporting a small readvance during the Younger Dryas itself [e.g., Clark and Gillespie, 1997; Menounos and Reasoner, 1997; Licciardi *et al.*, 2004]. Within these bounds, the details of the deglaciation histories of other glaciers are poorly known.

[22] Because the ARV glacier is over four times as long as the MBCV glacier, the mean rate of retreat was much higher in the ARV. This does not on its own mean that the rate of ELA rise was higher in the San Juan Mountains than in the Front Range; that can only be determined by accounting for the hypsometry of each valley. One way to do this might be to use an accumulation area ratio (AAR) method [e.g., Porter, 1975] to reconstruct ELA from each exposure age measurement site over the course of retreat. However, this approach involves the following two major assumptions: (1) that the AAR is constant at steady state regardless of the size and shape of the glacier within a valley and (2) that the AAR is some predetermined value, usually chosen from the literature, which stays constant through the retreat. Instead, we elect to use a numerical model to reconstruct each glacier on the basis of a simple set of climate parameters and the physics of ice flow. This approach allows us to relate ELA to glacier size without assuming an AAR, and to predict the effects of specific deglaciation histories on the cosmogenic record.

3. Numerical Model

3.1. Glacier Simulation

[23] We modified the GC2D numerical glacier model to predict cosmogenic nuclide concentrations in a glaciated valley for a given history of ELA change. The glacier model development is described in detail by Kessler *et al.* [2006]. In brief, the model simulates ice transport on a 2-D grid by internal deformation (using the shallow ice approximation), sliding, and avalanching. Mass balance at each grid cell is calculated according to its elevation and a specified mass balance-elevation gradient. The sum of the mass balance and net ice transport into each cell sets the rate of change of ice thickness. Sliding speeds are calculated using an attractor formulation

$$U_s = U_c e^{1 - \frac{z}{z_b}}, \quad (6)$$

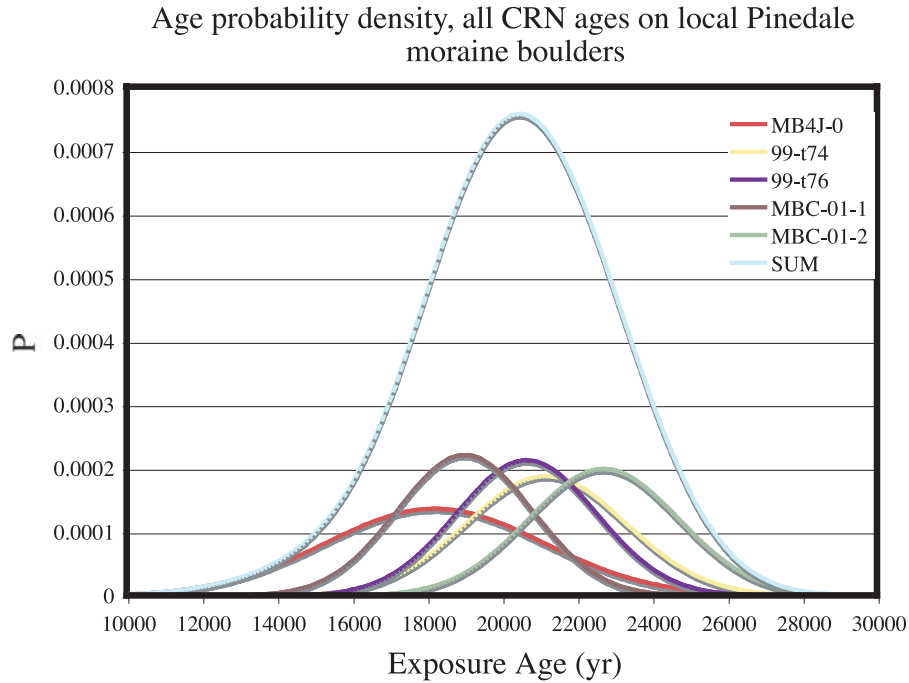


Figure 4. Probability density of all exposure ages of local Front Range Pinedale moraine boulders. The modal age is 20.0 ± 1.5 ka. See Table 1 for sample details.

where U_s is sliding speed, U_c is a typical sliding speed (here, 10 m/a), τ_c is a typical basal shear stress for temperate glaciers (10^5 Pa [Pierce, 1979]), and τ_b is the basal shear stress at each cell, calculated from ice thickness and surface slope. Advantages and disadvantages to this approach and others are discussed in the appendix of Kessler *et al.* [2006]. The model calculates erosion rate from sliding speed at each cell according to

$$\dot{E} = aU_s^b, \quad (7)$$

where \dot{E} is erosion rate, a is a scaling coefficient, and b is a power relating sliding speed to erosion (generally, $1 \leq b \leq 4$ [Harbor, 1992; MacGregor *et al.*, 2000]; here, $b = 1$). For this study, a is chosen so that the typical sliding speed U_c results in an erosion rate of 0.1, 1, or 10 mm/a, as these rates span the typical range for erosion by temperate glaciers [Hallet *et al.*, 1996; Loso *et al.*, 2004; Riihimaki *et al.*, 2005]. For $U_c = 10$ m/a and $b = 1$, a is correspondingly 10^{-5} , 10^{-4} , or 10^{-3} . Because we are concerned with the longitudinal pattern of erosion as it pertains to the erosion of CRNs, rather than the detailed 2-D erosion pattern, our results are relatively insensitive to the specific sliding and erosion formulations as long as geologically reasonable parameters are chosen.

[24] The mass balance profile increases linearly with elevation, crossing 0 at the ELA, until a cap at 2 m/a [after Anderson *et al.*, 2006]. In all model runs we employ a mass balance-elevation gradient of 10 m/a/km. All changes in glacier extent are therefore caused by changes in the ELA through model time. In practice, our model results and general conclusions are not affected by use of different, realistic mass balance profiles. In this application, we are not interested in the relative variations of precipitation and temperature that affect the ELA, but rather with how

changes in the glacier extent are reflected in the cosmogenic ages. Our discussion of climate change will therefore be expressed in terms of effective ELA history, assuming the mass balance gradient used here remains constant through deglaciation.

[25] For the assumed mass balance gradient, the terminal moraines and trimlines of MBCV are well matched by an ELA of 3350 m above sea level. This is higher than the AAR-based ~ 3160 m reported by Meierding [1982], but similar to the value reported by Brugger [2005] for the nearby Sawatch Range. MBCV is completely deglaciated when the model ELA rises above ~ 3900 m. The LGM glacier extent in the ARV is well matched with an ELA of 3100 m, and full deglaciation occurs here when the ELA rises above ~ 4000 m. In this valley, the modeled LGM ELA agrees well with Leonard's [1984] reconstruction on the basis of the AAR method.

3.2. Cosmogenic Production and Loss

[26] The latitude and altitude of each cell in DEMs of our study sites are used to generate a CRN production rate grid for each valley. The model applies the scaling of Stone [2000]. The production rate at each cell is also corrected for topographic shielding by an algorithm that first calculates the inclination of each point on the grid relative to each other point, and then finds for each cell the highest inclinations in 1° windows around the horizon. This horizon is then input to the CRONUS skyline calculator (available from <http://hess.ess.washington.edu/math/>), which returns a correction factor. Corrections in both valleys are small and are consistent with values calculated from skyline measurements made in the field at our sample locations. This set of scaling calculations allows the model to predict realistic CRN concentrations at each cell. In this paper, however, we present results normalized by the production rate at each

cell (i.e., we report model cosmogenic ages), rendering the model results insensitive to scaling details.

[27] During model runs, cosmogenic production is taken to be zero in areas covered by more than 10 m of ice. The CRN inventory at each cell can also decline because of glacial erosion. We compute an erosion rate \dot{E} as specified above, on the basis of local basal sliding speed, and calculate the reduction in CRN inventory by the depth stripped in each timestep:

$$N_e = N_0 e^{-\frac{\dot{E}t}{z_*}}, \quad (8)$$

where N_e is the posterosion inventory in the surface of the rock, N_0 is the preerosion inventory, dt is the model timestep, and z_* is the e -folding scale for cosmogenic production rate decrease with depth into rock (~ 60 cm for ^{10}Be). The depth of erosion at each timestep is also subtracted from the elevation of the cell in the digital elevation model (DEM).

[28] Once the model has “spun up” to steady state at the maximum glacial extent, an ELA history is imposed and the glacial response is calculated. We use a 1000 year spin-up time, although the glacier reaches its initial steady geometry within ~ 500 years. The extra time allows erosion to fully reset the CRN inventory accrued during the spin-up period (at the terminus, ~ 500 years worth).

[29] We simulate the glacial response to ELA histories that include: stepwise change, linear rise, and long-term linear rise scenarios that include short-term drops. Each scenario generates a pattern of exposure ages in the CRN layer that can be compared with the measured ^{10}Be ages.

4. Model Experiments

[30] Because the MBCV glacier was significantly smaller than that in the ARV (~ 20 km long versus ~ 90 km long), model runs complete much more quickly for MBCV. We therefore use this valley for the majority of our simulations. We simulate deglaciation of MBCV driven by monotonic and nonmonotonic ELA change histories, with varying efficiencies of glacial erosion. All scenarios begin at 22,000 model years BP, and the model is allowed to find a steady state during the first 1000 model years. At 21 ka BP, the history of ELA changes begins. The lowest ELA in any scenario is 3350 m, which creates a glacier that matches well the position of the terminal moraines. The highest ELA is more arbitrarily chosen to be 3900 m, approximately the mean elevation of the continental divide in this area. This insures full deglaciation of MBCV. Each scenario predicts a distinct pattern of exposure ages (Figure 5). After each model run, we extract age-distance profiles along the thalwegs of two major tributaries of MBCV (Figure 5, dashed lines); our results are presented as age-valley-distance profiles for each tributary relative to the terminal moraine.

4.1. Monotonic Retreat Histories and the Effect of Valley Hypsometry

4.1.1. Step Change

[31] The first scenario (Figure 6a, blue lines) is a stepwise rise in the ELA from its lowest value (3350 m) to its highest (3900 m). This results in complete deglaciation of MBCV

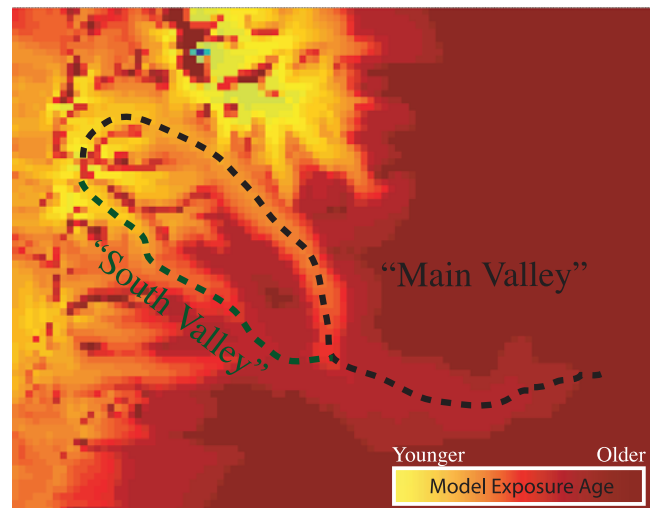


Figure 5. A typical model exposure age output grid. Redder colors are older exposure ages. Age versus valley distance profiles are extracted from the exposure age grid after each model run for each of two tributary valleys in the MBCV. Profile locations are determined using a channel extractor, i.e., profiles correspond to the thalweg of each valley.

within a few hundred years (Figure 6b). Importantly, this demonstrates that the response of these glaciers to a change in ELA is very rapid, and that short-term fluctuations around a long-term ELA rise should elicit a response.

4.1.2. Linear ELA Rise

[32] Two linear ELA rise scenarios (Figure 6a, red lines) result in monotonic age-distance relationships, with minor variability due to the detailed hypsometry of the valley (Figure 6b). We emphasize that the retreat rate varies under steady ELA rise due solely to the hypsometry of the valley. The only difference between the scenarios is the rate of ELA rise; the age-distance curves differ only in their slope. Because of differences in hypsometry between the MBCV southern tributaries and the northernmost, the southern tributary glaciers retreat farther up their valleys for a given ELA rise than does the northern glacier. In other words, the south valley glacier “disconnects” from the trunk glacier before the trunk glacier retreats past the tributary junction. This results in an area above the tributary junction in the southern valley that is exposed for much longer than the part of the northern valley near the tributary junction. This is manifested as an up-valley increase in ages in the south valley at the tributary junction. The discrepancy in the ages at equivalent positions along each valley increases with the slope of the age-distance trend. This is because, in a slower retreat, the bed of the south tributary is exposed for a longer time before the equivalent position in the northern tributary is exposed.

4.1.3. Linear Rise With an Embedded Protracted Stillstand

[33] A third type of monotonic deglaciation includes a period of stillstand in the midst of the long-term retreat (Figure 7a). The effect of such a history is to produce a step in the age-distance trend, with the initiation age of the stillstand represented by the upper lip of the step and the end

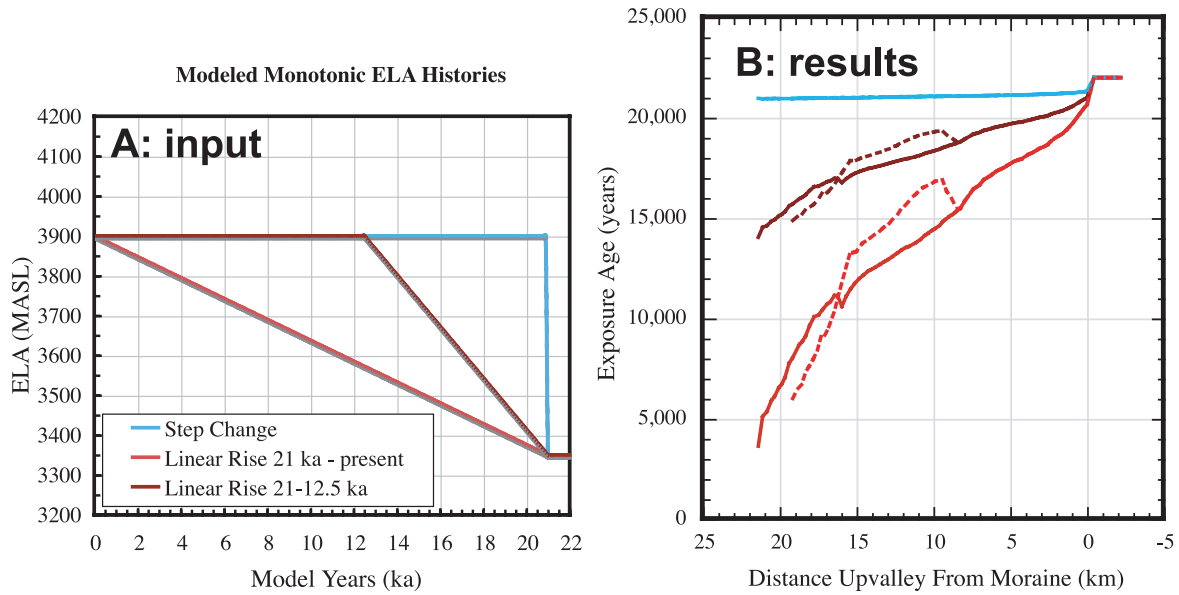


Figure 6. (a) Modeled monotonic linear ELA rise histories and (b) resulting age-distance trends for MBCV. In Figure 6b, down valley is to the right, and the dotted lines represent results for the MBCV south tributary. The step change scenario (blue line) results in nearly immediate deglaciation of the entire valley. Progressively slower ELA rise histories (dark and light red lines) result in progressively steeper age-distance trends. Note that the discrepancy between the exposure ages in the two tributaries, due to detachment of the tributary from the trunk glacier, is enhanced by slower rates of retreat. The discrepancy exists because the hypsometry of each tributary is different, meaning that the elevation distribution in the accumulation area of each tributary is different. The up-valley increase in age in the south valley at the tributary junction is a result of this effect, as is the small inflection at 16 km in the main valley, where two smaller ice streams merge.

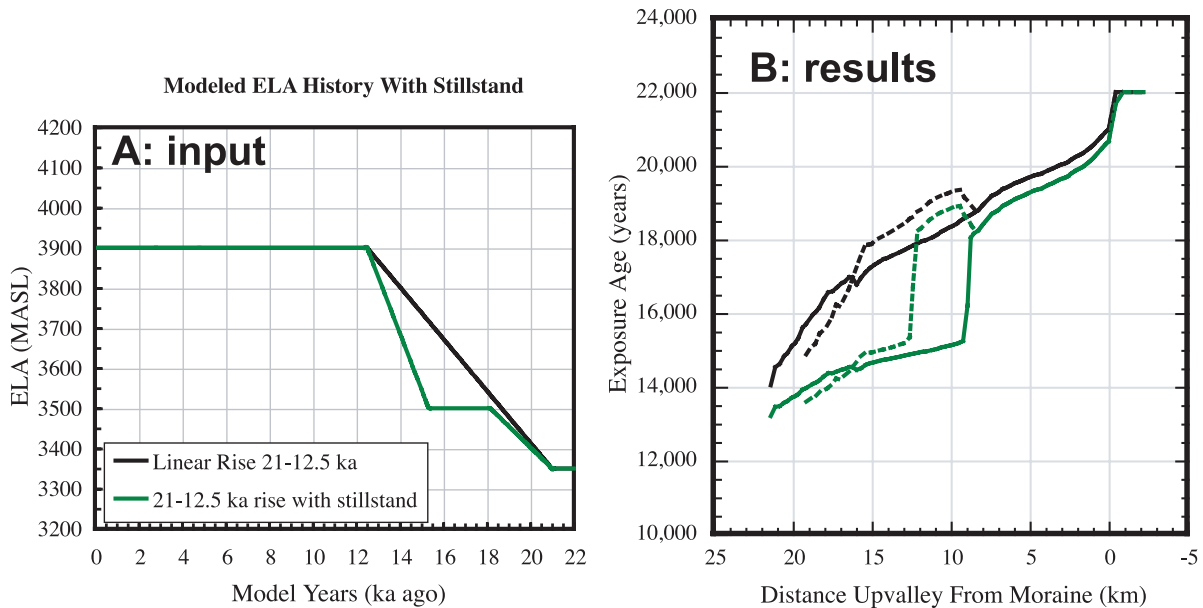


Figure 7. (a) Modeled monotonic ELA rise history including a period of stillstand and (b) resulting age-distance trend for MBCV. In Figure 7b, down valley is to the right, and the dotted lines represent results for the MBCV south tributary. We replot in black the results from the 21–12.5 ka linear rise scenario for comparison (see Figure 6). The stillstand results in a dramatic step in the age-distance trends for both tributaries. The discrepancy between the exposure ages in the two tributaries is greatly enhanced in this case because the stillstand occurred after the two tributaries detached.

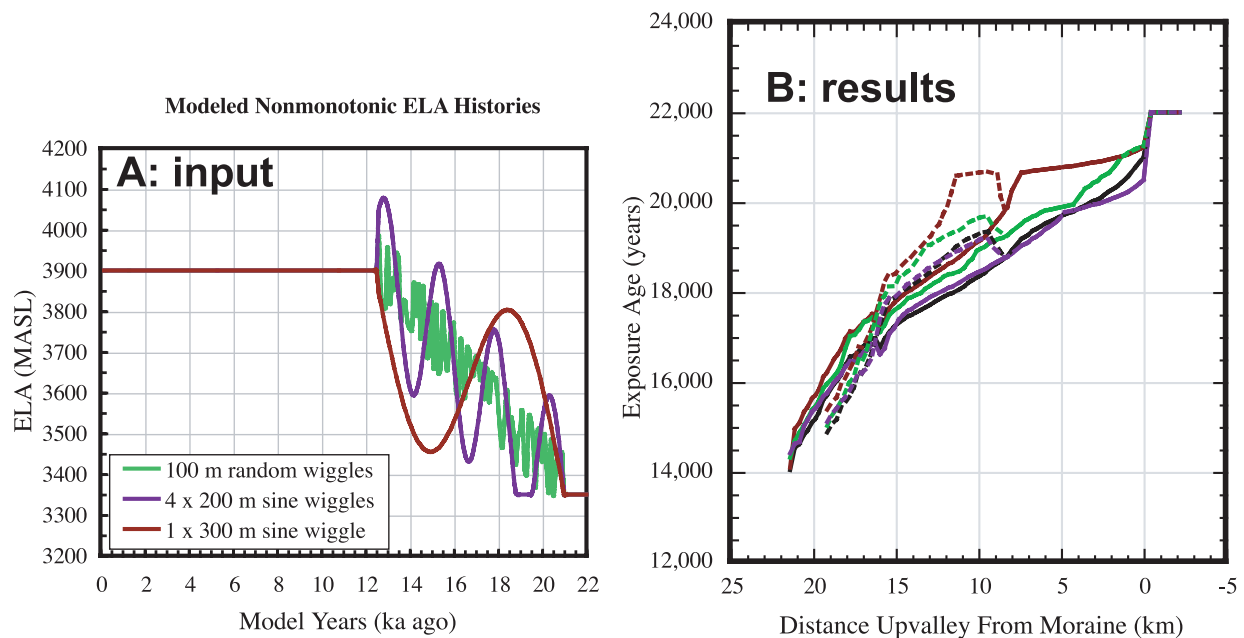


Figure 8. (a) Modeled nonmonotonic ELA rise histories (i.e., including short-term readvances) and (b) resulting age-distance trends for MBCV, with zero erosion during readvances. In Figure 8b, down valley is to the right, and the dotted lines represent results for the MBCV south tributary. Black lines in Figure 8b are the replotted results from the 21–12.5 ka linear rise scenario for comparison (see Figure 6). Only when the ELA oscillation is of sufficient duration (>3 ka) and amplitude (in this case, 300 m) do the age-distance trends differ significantly from the baseline linear ELA rise case, when erosion during readvances is not accounted for. In Figure 8a, ELA histories were truncated at 3350 m, the ELA that replicates the glacier’s LGM extent.

of the stillstand dated by the base of the step (Figure 7b). These steps are seen in the age-distance trends of each tributary, and their position depends on the location of the terminus in each tributary at the time of the stillstand. If the stillstand occurred after detachment of the tributary from the main glacier, this results in a large discrepancy between the exposure ages of the tributaries just above their junction. The age discrepancy is approximately the duration of the stillstand.

4.2. Retreat Histories Including Readvances: No Erosion

[34] The cosmogenic age patterns resulting from retreat histories that include readvances differ from monotonic retreats for the following two reasons: (1) the exposure history at each site includes periods of zero CRN accumulation after initial exposure and (2) erosion during readvances can partially or totally reset the cosmogenic signal acquired during initial retreat. These separate effects may have different relative importance depending on the setting. Here, as before, we use the GC2D model to explore the impact of each of these effects on a generic exposure age-distance trend.

[35] In one set of experiments, we turned off erosion in the model and drove the glacial response with a variety of ELA rise scenarios that include readvances. This tested the effect of readvances on the cosmogenic record via modification of the exposure history, independent of the effect of erosion. For these scenarios, we used as a baseline a linear ELA rise from 3350 m at 21 ka to 3900 m at 12.5 ka. To this

we added short-term oscillations of varying amplitude and wavelength. The details of each scenario are described below and are shown in Figure 8.

4.2.1. The 100 m Random Wiggles

[36] In this experiment, random variation of 100 m maximum amplitude (amplitudes drawn from a uniform distribution) and high frequency (~ 200 years) was added to the baseline ELA rise history. This caused the model glacier to advance and retreat frequently and quickly throughout the overall retreat. The resulting age-distance trend did not differ significantly from the baseline case (Figure 8). Overall, ages are slightly older in this specific case than in the linear case, because up-valley sites are exposed earlier in the retreat history than in the linear case. The discrepancy depends on the details of the random fluctuations, but is always smaller than typical cosmogenic dating errors. This implies that such short-term variation in climate, though clearly felt by the glacier, will not be resolved using the CRNs in polished bedrock method.

4.2.2. The 4 \times 200 m Sine Wiggles

[37] Four sinusoidal ELA oscillations of 200 m amplitude and ~ 2500 year period caused bigger, longer-term advance-retreat cycles during deglaciation. The resulting age-distance pattern was again indistinguishable from that given by the baseline linear retreat.

4.2.3. The 1 \times 300 m Sine Wiggle

[38] One sinusoid of 300 m amplitude (rising at 21 ka, falling between ~ 18.5 and 16 ka, then rising to 3900 m and leveling at 12.5 ka) creates an extensive, rapid retreat, readvance, and final fast retreat. This scenario predicts a

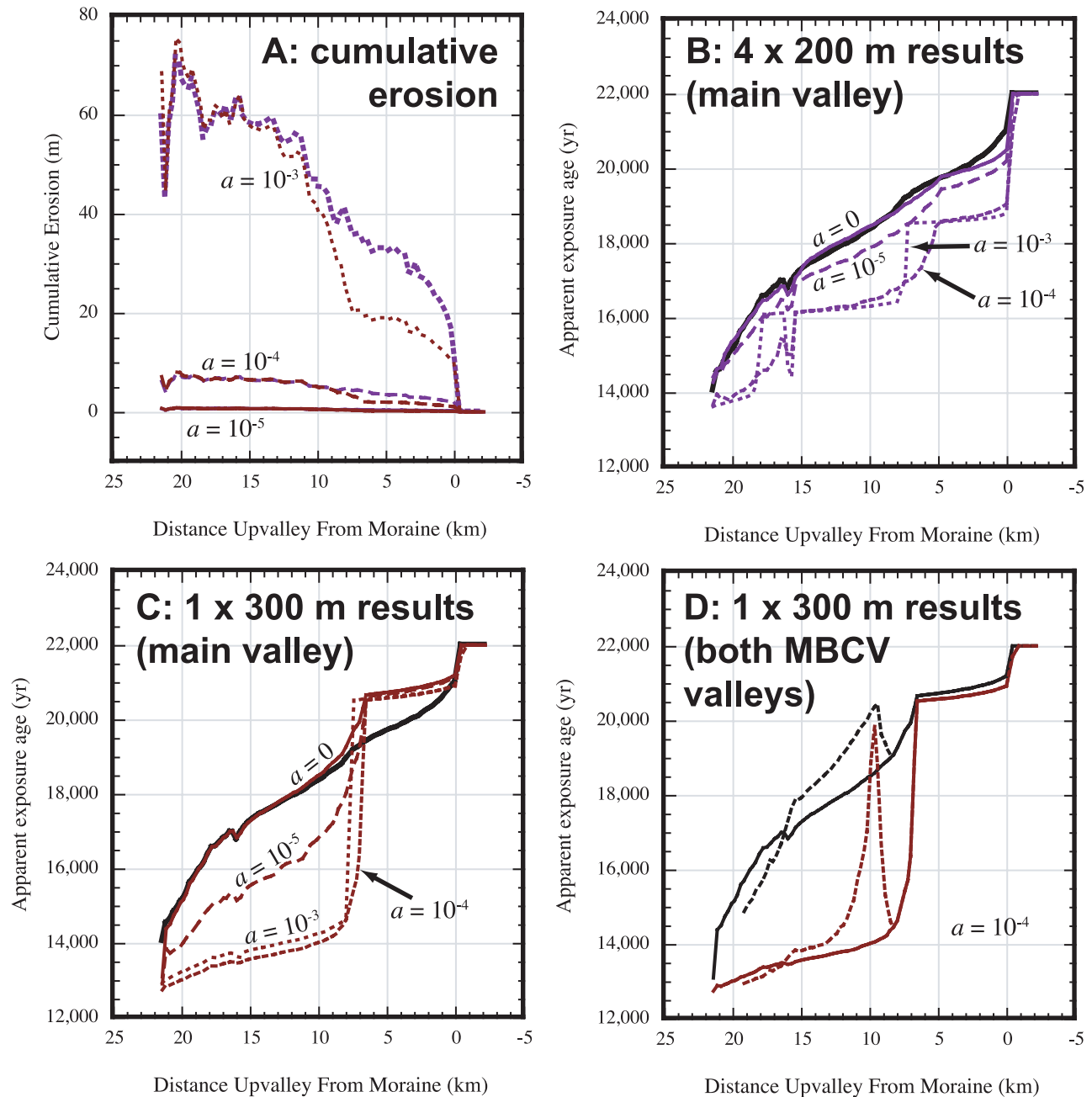


Figure 9. (a) Modeled cumulative erosion for different values of the erosion coefficient a (equation (7)) during nonmonotonic ELA rise histories (colors as in Figure 9a). (b–d) Resulting age–distance trends for MBCV. Black lines in Figures 9b–9d are the replotted results from the 21–12.5 ka linear rise scenario for comparison (see Figure 6). In Figures 9b and 9c, all results are for the MBCV main valley, and dashed lines represent different erosion rates. In Figure 9d, the large-amplitude oscillation case is plotted for both tributaries (with the dashed line being for the south valley) for the ~ 1 mm/a erosion case ($a = 10^{-4}$ in equation (7)). Erosion during readvances results in steps in the age–distance profiles at positions corresponding to the terminus position during each readvance. Greater modification to the age–distance trend is a result of longer-duration oscillations and higher erosion rates. However, rates above ~ 1 mm/a effectively reset CRN exposure ages even during a short readvance, so rates higher than this do not further affect the age–distance trends.

different pattern of ages in the bedrock than does the baseline linear ELA rise (Figure 8b). Specifically, this scenario results in systematically higher ages in the lower parts of the main valley and the south tributary, which were

not reoccupied during the readvance. Had these sections been reoccupied, the results would be more similar to those of the linear case. This means that the details of the age–distance trend are indeed sensitive to the details of the

retreat-readvance history, particularly the magnitude and duration of the readvance.

4.2.4. Summary of No Erosion, Nonmonotonic Experiments

[39] When erosion is not considered, exposure age-distance trends begin to differ significantly from those given by linear ELA rise only when the ELA oscillations occur on a timescale of about ~ 4 ka and the ELA oscillation amplitude is ~ 200 – 300 m. Practically, this means that histories are distinct when the retreat/advance distance amplitude is a large fraction of the valley length, and when readvances occur over a timescale that is roughly twice the error limit for cosmogenic dating.

4.3. Effect of Erosion During Readvances on the Age-Distance Trend

[40] We assessed the effect of erosion during readvances on the age-distance trend by extracting both actual time of exposure (tracked by the model) and apparent CRN exposure age (modified by erosion) along the same longitudinal transects of the valley as above (Figure 9). We did this for the ELA scenarios with 4×200 m and 1×300 m sine wiggles. Not surprisingly, the amount and style of age-distance trend modification scales with the duration and extent of readvances. In both modeled cases, age-distance transects are strongly modified by erosion when erosion rates are scaled to be $\geq \sim 0.1$ mm/a (i.e., in equation (7), $a \geq 10^{-5}$). Erosion rates higher than ~ 1 mm/a ($a \geq 10^{-4}$) yield equivalent results because, once the cosmogenic age at a point is reset to zero, subsequent erosion cannot reduce it further.

[41] The overall pattern that results is a flattening of parts of the age-distance trend into steps, with the “risers” corresponding to the maximum terminus position during each readvance. This step-flat morphology of the age-distance trend is a signature of readvances during deglaciation. Brief readvances do not affect the exposure ages as much as protracted readvances because insufficient time is available to erode the bed. A readvance that fully resets exposure ages within its extent gives an equivalent pattern to a protracted stillstand at an equivalent down-valley extent. This is not the case if the readvance only partially resets ages, which depends on the erosion rate and duration of the readvance.

5. Application of Model Results to Cosmogenic Deglaciation Records From the ARV and MBCV

5.1. Utility of the Model ELA-Age Relationship

[42] As we demonstrated above, valley hypsometry affects the rate of glacier response to a given change in ELA, and different tributaries with differing hypsometries therefore respond differently to the same forcing. To understand our cosmogenic record of retreat in the context of climate change, we must remove this hypsometric effect. To do this we constructed a diagram in which each cosmogenic sampling site is related to the ELA that best recreates the glacier with its terminus at that site.

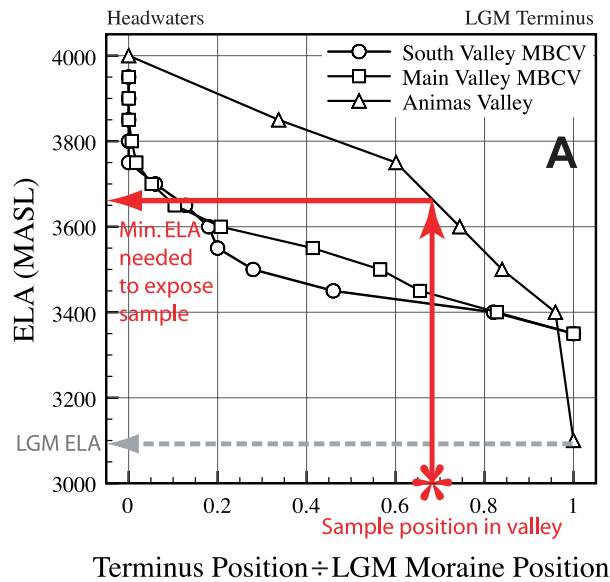
[43] We began by simulating a stepwise lowering of the ELA in 25 m intervals, allowing 500 model years between steps for the glacier to come to equilibrium. This allowed us to characterize the relationship between ELA and equilibrium

glacier terminus position for each valley (Figure 10a). From this, we constructed an ELA-age diagram by picking the ELA that corresponds to the terminus valley position at each sample (Figure 10a). This is plotted against the sample age (Figures 10b and 10c). The ELA-age graph represents the monotonic (but not necessarily linear) ELA history that most directly matches the terminus retreat history constrained by the cosmogenic age dates.

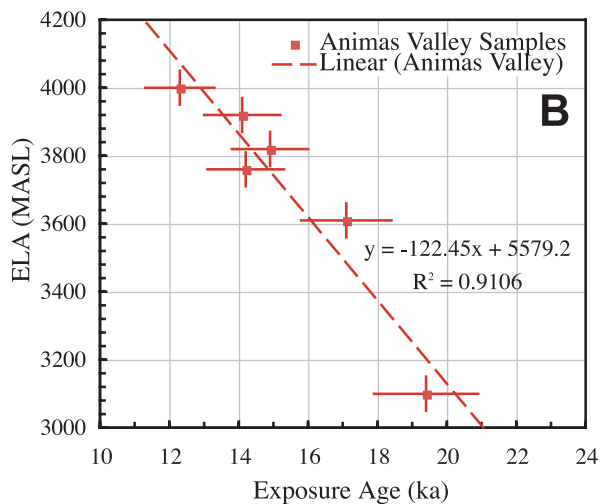
[44] We note that this could be accomplished using an AAR method, wherein an assumed AAR is used to determine the ELA for each terminus position. However, this requires that an AAR be chosen, and that this chosen AAR is constant regardless of the size or shape of the glacier. This latter assumption is probably incorrect. The GC2D model predicts an AAR of 0.59 for the MBCV glacier at its LGM position, which is consistent with AAR values commonly used in glacier reconstructions ($\sim 0.60 \pm 0.05$ [Porter, 1975]). However, for MBCV, the steady state AAR declines as the glacier becomes shorter (Figure 11). We hypothesize that this is again related to the hypsometry of the valley, for several reasons. Shorter glaciers are entirely contained on steep slopes in the upper valley. Steeper slopes promote faster ice flow and more efficient mass transfer into the ablation zone, reducing the relative accumulation area needed to maintain a glacier of a particular size. The typical shape of a glacial valley is also quite wide in the headwaters, where several cirques occur, and narrows considerably once these tributaries converge. The result is that glaciers that are confined to the headwaters tend to have lower AARs than those that extend well down valley past major tributary junctions.

[45] One of the useful properties of the ELA-exposure-age diagram is that hypsometric effects are accounted for; we have converted a temporal record of terminus position to a temporal record of effective ELA (which represents the climatic forcing history). For the Animas Valley, this has the effect of removing the apparent acceleration in deglaciation seen near 14 ka (Figure 10b; cf. Figure 3). In the Animas Valley, a linear regression through the ELA-age data passes through the 1σ errors of all samples with an R^2 value of 0.91 for an ELA rise rate of 122 m/ka. The acceleration seen in the raw retreat history is likely the result of valley hypsometry, and does not imply an increase in the ELA rise rate at that time.

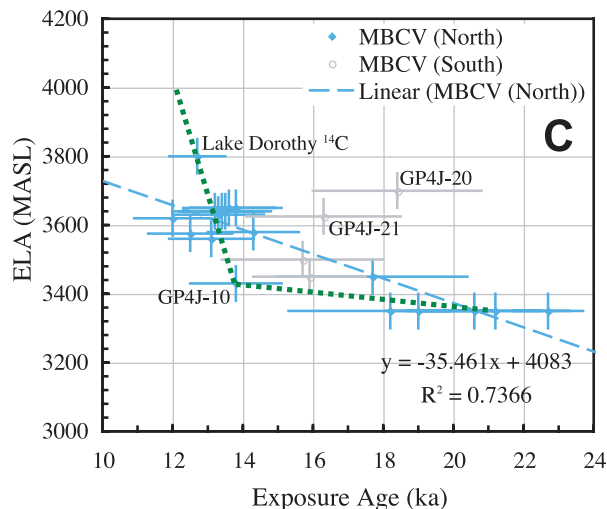
[46] Because hypsometry is accounted for, exposure ages from different tributaries of the same valley should fall into the same monotonic trend in ELA-age space, assuming that all tributaries experienced the same climate forcing. This should be true if the tributaries are relatively large and similar in topographic aspect; small cirque glaciers are more sensitive to local differences in temperature, wind redistribution of snow, and insolation. Data for the main and south tributaries of MBCV can be connected with a single monotonic trend on the ELA-age plot, with a few outliers (Figure 10c). A negative ELA-age slope (i.e., ELA apparently decreasing with time) among samples from a given tributary must reflect the presence of inheritance among some samples, because the CRN ages record only total time of exposure. This is not necessarily detectable in an age-distance trend, because ages can increase up valley at tributary junctions because of “disconnection” of the tributary during retreat. Because this is a hypsometric effect,



Model ELA vs. CRN age



Model ELA vs. CRN age



it is removed in ELA-age space, and all tributary ages should plot along the same ELA rise history. Our sample GP4J-20, for instance, plots well above the trend occupied by all other points from MBCV (Figure 10c); we therefore interpret it to contain a cosmogenic inventory that was not fully reset during the last glacial cycle. Similarly, samples that plot in isolation below the main trend may have been more greatly affected by snow or sediment shielding than were the bulk of the other samples (for example, GP4J-10). In effect, this allows us to isolate these confounding effects in specific samples.

5.2. Interpretation of the MBCV Deglaciation Record

[47] We used the ELA-age diagram for MBCV to construct plausible ELA rise histories on the basis of the cosmogenic ages. Each history was then used to drive the model, and the predicted age-distance trends were compared to the measured age-distance trend. The simplest ELA history is a linear fit to the ELA-age data (Figure 10c). For the MBCV, this fit suggests a rise rate of 35 m/ka, with an R^2 of 0.75. Note that it does not pass through the radiocarbon age in the upper cirque, but can account for much of the CRN data in both tributaries. When driven with this ELA rise, the model predicts a steadily decreasing age-distance trend (Figure 12), with a ~ 1.5 ka exposure age difference between the main and south tributaries in a several km long reach above the junction. This history overpredicts ages in the mid-main valley by ~ 2 ka, as is apparent on the ELA-age plot.

[48] A nonlinear monotonic fit (by eye; slow ELA rise until 13.8 ka, then quick and total deglaciation by 12.5 ka; see Figure 10c) passes through the bulk of the CRN data as well as the radiocarbon age. This scenario results in a model age-distance trend that displays a rapid drop in age with distance up valley of the moraine, and then flattens (Figure 12). This fits the upper main valley well, but underpredicts the lower valley age by almost 4 ka. It also predicts no difference between tributary ages because of the fast, late retreat; in other words, it underpredicts south valley ages by ~ 2 ka. That both of these histories fail to match a significant portion of the data suggests that a period of stillstand or readvance is needed in the deglaciation history.

Figure 10. (a) Steady state terminus positions versus ELA for MBCV. These curves can be used to construct a (b and c) baseline ELA history from the position and age of CRN exposure samples. These relationships are derived from steady state terminus positions. Figure 10b is the ARV ELA-age plot. A linear ELA rise from 20–12 ka explains the cosmogenic ages very well. Figure 10c is the ELA-age plot for MBCV. Within error, all data from both tributaries should be connected by a single monotonic path. Because they are not, some samples must include inheritance (e.g., GP4J-20 and -21) or an unusual shielding history (e.g., GP4J-10). The green dotted line is an arbitrary, nonlinear, monotonic ELA history that fits most of the main valley data but underpredicts all south valley ages (see resulting age-distance trend in Figure 12). Error bars on ages include 1σ analytical uncertainty and production rate scaling uncertainty.

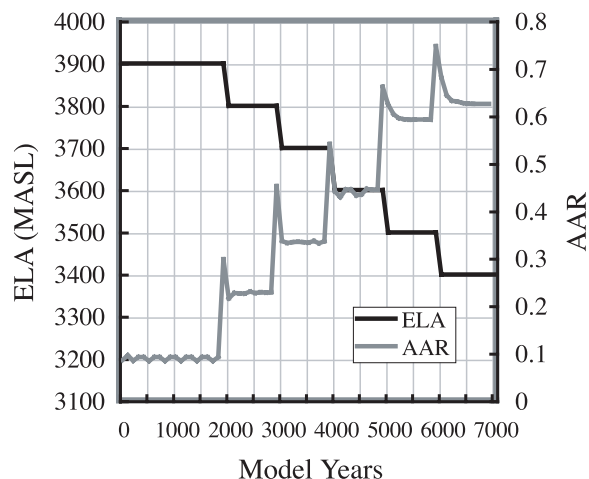


Figure 11. Modeled AAR versus ELA for MBCV in an experiment in which ELA was lowered in 100 m steps. Note the transient AAR spike coincident with each step, followed by an equilibration to a steady AAR after a few hundred years. As the glacier approaches its LGM extent (ELA = 3350), the equilibrium AAR converges to ~ 0.6 . However, higher ELAs result in much lower AAR values. This behavior is symmetric, that is, stepping up to an ELA results in the same AAR as stepping down to that ELA. This means that the GC2D model and the AAR method will disagree greatly in glacier reconstructions for this valley when the glacier is much shorter than its LGM extent.

[49] Construction of a compatible history with a readvance or stillstand requires careful examination of both the ELA-age plot and the age-distance plot of the measured ages. Because of the plateau of similar ages in the upper to middle main valley, the final retreat is constrained to occur between 14 and 12.7 ka. The initial retreat must pass the lower valley at ~ 18 ka and the mid-south valley at about 16–17 ka to explain the older ages there. Any readvance cannot extend much past the tributary junction in the main valley and cannot cause erosional resetting of the lower and middle south valley ages (otherwise these ages would be ~ 14 ka, reflecting the final retreat). Given these constraints, erosion rates scaled to ~ 1 mm/a ($a = 10^{-4}$), and a bit of trial and error, we arrived at two ELA histories that fit the majority of our exposure ages (Figure 13). The first of these contains a partial readvance beginning at 15.5 ka. The other is similar, but with a stillstand between 16.0 and 13.8 ka instead of a readvance. The resulting age-distance trends (Figures 13b and 13c) replicate well the measured CRN ages throughout the main valley, including the ~ 3 ka step in ages just below the tributary junction. They also match the increase in exposure ages in the south valley just above the tributary junction. In both cases, it is difficult to create a single history that passes through both GP4J-10 and GP4J-21 (ignoring GP4J-20; see above); tailoring the history to one causes us to miss the other. This can be seen easily on the ELA-age plot (Figure 10c), as a single monotonic history in ELA-age space cannot pass through both of these points. It is possible to include both (at the ends of their error bars) if the cosmogenic inventory acquired at GP4J-21 during initial retreat was only partially reset during the readvance. Thus, these histories are not

unique, given our poor constraint on erosion rates and their scaling with glacier size. However, any history constructed must obey the constraints we have discussed above, and so cannot vary too much even if erosion rates during the readvance are different from the ~ 1 mm/a we assumed for these reconstructions.

6. Discussion

[50] The spatial pattern of CRN concentrations in a deglaciated valley ultimately depends on three factors: the ELA-terminus position relationship (as determined by valley hypsometry), the time distribution of terminus position, and the rate of glacial erosion. Absent erosion, any two statistically similar ELA time histories will yield similar exposure age patterns in a particular valley. The details of a given history matter where erosion is important to modifying the CRN signal, i.e., where erosion rates exceed ~ 0.1 mm/a. Differences in hypsometry between tributary valleys result in different responses to the same changes in local climate. Specifically, periods of steady retreat result in age differences between tributaries of differing hypsometry that scale inversely with the rate of retreat. During non-monotonic retreats, exposure ages also differ between tributaries depending on the extent and duration of readvances, and the erosion rate of the glacier during these

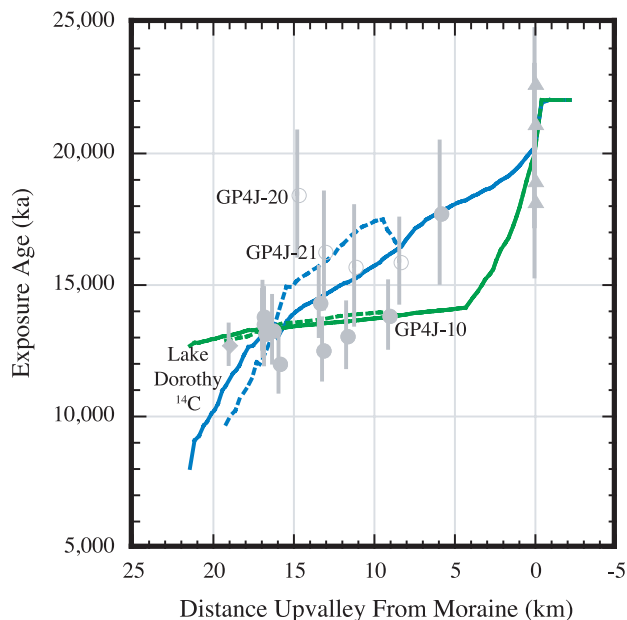
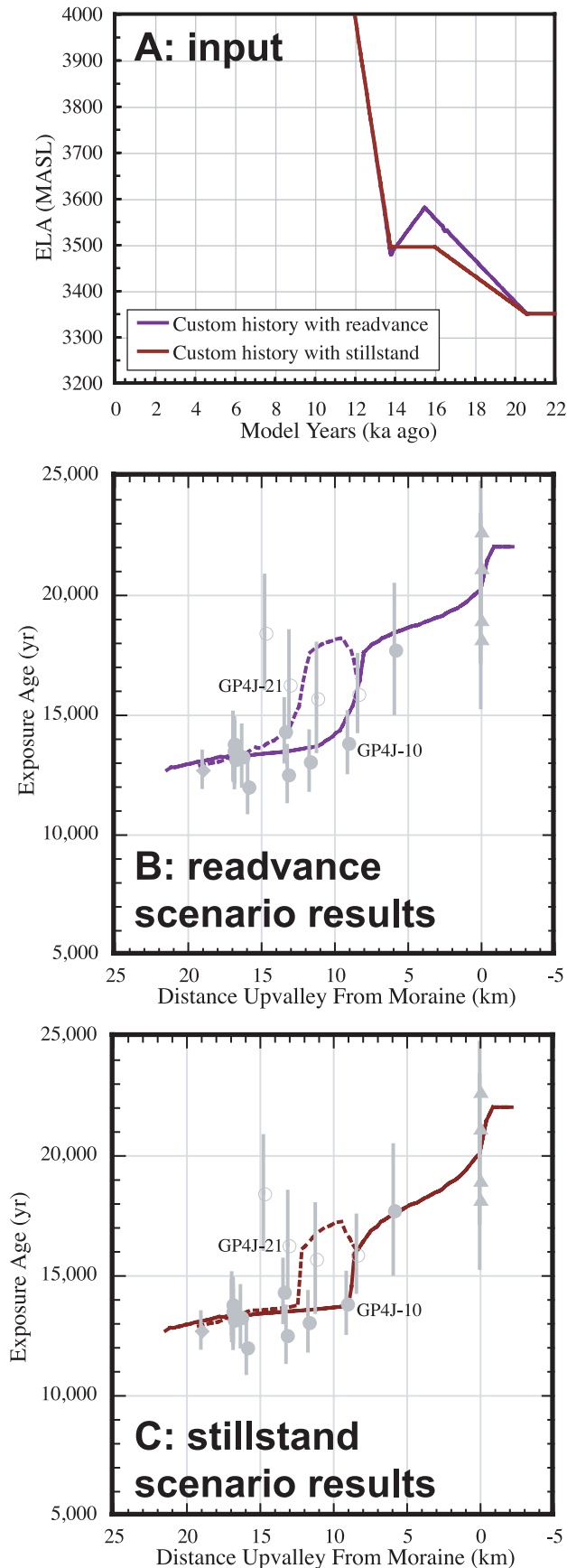


Figure 12. Model age-distance trends for MBCV resulting from the histories drawn from the ELA-age plot (Figure 10c). Gray data points are the CRN and radiocarbon age data (symbols as in Figure 3). Open symbols and dashed lines represent the south tributary. The linear fit (blue line) overpredicts exposure ages through the middle of the main valley but fits the headwaters, lower valley, and south valley well. The arbitrary nonlinear history (green) results in a better fit to much of the main valley data but greatly underpredicts the south valley ages. Labeled samples are discussed in the text. Error bars on ages include 1σ analytical uncertainty and production rate scaling uncertainty.



readvances. Because of these differences, the details of the age patterns among two or more tributaries of the same glacial valley can be used to place rigorous constraints on the deglaciation history of that valley. The ELA-terminus position relationship can be used to plot the CRN samples in ELA-age space. This allows the CRN age data to be viewed without hypsometric effects, ties the deglaciation history to climate, and allows detection of samples that either contain inheritance or have been shielded by sediment or snow to a greater degree than other samples.

6.1. Implications for Regional Climate Following the LGM

[51] LGM ELAs in WNA were generally lower than modern values by ~ 600 – 1000 m, but this varies from location to location [Pierce, 2003; Kaufman *et al.*, 2003]. LGM ELAs were lower in northern and more coastal areas and higher in the interior and to the south [Porter *et al.*, 1983]. Our model results imply a 900–1000 m lower ELA at the LGM in the Animas River Valley and at least 600 m lower in Middle Boulder Creek Valley. On the basis of the ELA-age relationships in both valleys, the mean rate of ELA rise was significantly higher in the San Juan Mountains than in the Front Range. This prompts the question of whether this is a local effect or if a systematic trend in ELA rise rate can be seen from north to south in the Rocky Mountains. We point out that the total ELA change between LGM and deglaciation was necessarily greater in the San Juan Mountains than in the Front Range, because the LGM ELA was probably lower in the ARV than in MBCV, and a higher ELA is needed to fully deglaciate the ARV. As there is more high-elevation terrain in the San Juan Mountains than in the Front Range, they are not deglaciated until the ELA reaches ~ 4000 m, whereas an ELA of 3900 m deglaciates MBCV. Regardless, the exposure ages from the ARV are well explained by a steady ELA rise history, with no acceleration, stalling, or readvance. Short periods of stillstand or readvance (<1 – 2 ka long) might have occurred in this valley and would not be detectable using the methods discussed here.

[52] In contrast, the model results discussed above for MBCV suggest that a protracted (≥ 2 ka) partial readvance or stillstand occurred in the Front Range between initial deglaciation at ~ 21 ka and rapid deglaciation beginning at ~ 14 ka. This event did not leave a moraine record, and we can only speculate as to the reason. A quick readvance would likely leave less of a moraine than a slow one, and in both cases the moraine would be smaller than that left by a protracted stillstand. To explain the majority of our CRN ages, a stillstand would need to have been at least 2000

Figure 13. (a) Modeled customized ELA rise histories and (b and c) resulting age-distance trends for MBCV. ELA histories were customized after careful review of generic model results (Figures 7–10) and the ELA-age plot (Figure 11). Both scenarios satisfy most of the data from both tributaries and represent our preferred interpretations of the cosmogenic record from MBCV. Labeled samples are discussed in the text. Error bars on ages include 1σ analytical uncertainty and production rate scaling uncertainty.

years long. We can appeal to information from the adjacent valley to the north of MBCV. Here, the LGM glacier in North Boulder Creek Valley impounded ice marginal Lake Devlin ~ 3 km up valley of the Pinedale (LGM) moraines. Radiocarbon and OSL constraints from lake sediments indicate that the lake existed from ~ 23 to 14 ka, with the possibility of an outburst and subsequent reimpoundment ~ 15.5 ka [Madole, 1986; Leopold and Dethier, 2007]. One could interpret this to reflect a retreat of the glacier past the lake outlet and a subsequent readvance, which would be generally consistent with our timing from MBCV. We therefore tentatively suggest that a readvance is the more likely scenario in MBCV, but emphasize that both the stillstand and readvance scenarios explain the CRN data.

[53] In the northern U.S. Rocky Mountains, glaciers retreated from their last maximum positions at 16–17 ka [Licciardi *et al.*, 2001, 2004; Munroe *et al.*, 2006; Refsnider, 2008], suggesting that an advance at this time overrode any older, LGM-equivalent moraines in these valleys. A similar readvance in the southern Rockies has not been as well documented; if it occurred, it did not always override the 20–21 ka moraines. For example, terminal moraines with both LGM ages and ~ 17 and ~ 15 ka ages are found in the northern Sawatch Range, ~ 100 km southwest of MBCV [Schildgen, 2000; Brugger, 2005; Briner, 2007].

[54] Licciardi *et al.* [2004] proposed that the lengths of LGM alpine glaciers were suppressed in the north by the presence of the Laurentide Ice Sheet (LIS), and implied that glaciers across the United States Rocky Mountains regrew to their LGM positions or beyond at 16–17 ka because of a widespread cooling event at this time. Superimposed on this record was the reduction of the LIS and the corresponding northward shift of the jet stream. Our deglaciation record from MBCV corroborates a widespread readvance at about the same time, but it is constrained to lie within the LGM footprint. We hypothesize that the reduced orographic and thermal effect of the LIS by 16–17 ka allowed alpine glaciers in the north to regrow to or beyond their LGM limits, while more southerly glaciers only readvanced within their LGM footprints. Local effects, such as the presence of a nearby moisture supply as in the Uinta Mts. [Munroe *et al.*, 2006] or the differing response time of different ice streams as in the Yellowstone ice complex [Licciardi and Pierce, 2008], would have also affected the magnitude of this readvance relative to the LGM footprint. It is tempting to suggest, on the basis of the timing, that such a readvance was the result of widespread atmospheric cooling at mid-high latitudes following shutdown of North Atlantic deep-water circulation during Heinrich Event H1 [e.g., Clark and Bartlein, 1995; Benson *et al.*, 1996; Hostetler and Bartlein, 1999]. We note that the mechanism for any transmission of the North Atlantic signal to the rest of the world is not fully understood [Hostetler *et al.*, 1999], but the broad interhemispheric synchronicity of alpine glacier moraine deposition ~ 16 –17 ka is compelling [Schaefer *et al.*, 2006]. Farther south, our ARV exposure ages do not require a readvance or stillstand between the global LGM and full deglaciation, but this does not preclude the existence of a short-lived or small-amplitude readvance during this time. All of the studies cited above indicate rapid, extensive deglaciation across WNA between 14 and 12.5 ka (i.e., during the Bølling-Ållerød warming of the North Atlantic), with no

evidence for extensive glacier regrowth during the Younger Dryas.

6.2. Practical Advice for Applying the Methods of This Study

[55] The techniques discussed in this paper can be employed to provide an additional constraint on the deglaciation histories of individual alpine valleys where glacially polished bedrock suitable for cosmogenic dating can be found. Used in conjunction with radiocarbon, moraine exposure ages, and other constraints, they can help provide a more complete picture of the demise of alpine glaciers following the LGM. They are particularly useful where little evidence of glacial position is recorded between the LGM terminal moraine and the headwaters. We therefore conclude with some practical advice for efficiently applying these methods.

[56] Before sampling, a dynamic glacier model should be used to constrain the relationship between ELA and terminus position for all tributaries of the valley of interest. Reaches of tributaries that differ greatly in their ELA-terminus position curves should be prime targets for sampling, because these areas are where the greatest age discrepancy will result for a specific deglaciation scenario. These areas will therefore provide the strongest leverage on extraction of the deglaciation history. Ideally, several tributaries that join the main valley at different down-valley distances can be used. Very small tributaries should generally be avoided because they are more prone to topographic aspect and other local climatic effects, violating the assumption that all tributaries share a common forcing signal. Very small tributaries with low ice discharge and the highest headwaters of all tributaries are also less likely to be cosmogenically reset because of limited erosion in these settings [Anderson *et al.*, 2006].

[57] Densely spaced samples along the length of each valley will always be ideal. Because this is not always economical, we suggest emphasis on sites just above tributary junctions and in the main valley below each junction, on the terminal moraine, and in the headwaters. If radiocarbon or other independent constraint on deglaciation timing in the headwaters can also be obtained, it will provide a strong test of whether cosmogenic inheritance is a problem in a given setting.

[58] Once age data are obtained, it is important to use the ELA-terminus position curves to construct an ELA-age diagram. Data from all tributaries should generally collapse into one monotonic path in ELA-age space. Outliers may represent sites with inheritance (if high) or unusual shielding conditions (if low). This monotonic path will place strong constraint on the ELA histories that can explain the cosmogenic data, and the potential for details such as readvances and stillstands can be assessed in the context of this basic history.

[59] **Acknowledgments.** This research was partially supported by a grant from the NSF (EAR-0719902 and EAR-0724960). We thank Mark Kessler for repeated consultation about the glacial model development. Taylor Schildgen graciously provided raw data from her B.S. thesis. Maureen Berlin, Brian Clarke, Miriam Dühnforth, and Nora Matell assisted in the field and contributed through many enjoyable discussions. We thank S. Gupta, B. Phillips, and an anonymous reviewer for their critical comments on an earlier version of this paper.

References

- Anderson, R. S., P. Molnar, and M. A. Kessler (2006), Features of glacial valleys profiles simply explained, *J. Geophys. Res.*, *111*, F01004, doi:10.1029/2005JF000344.
- Andrews, J. T., P. E. Carrara, F. B. King, and R. Stuckenrath (1975), Holocene environmental changes in the Alpine Zone, northern San Juan Mountains, Colorado: Evidence from bog stratigraphy and palynology, *Quat. Res.*, *5*(2), 173–197.
- Balco, G., J. O. Stone, N. A. Lifton, and T. J. Dunai (2008), A complete and easily accessible means of calculating surface exposure ages or erosion rates from ^{10}Be and ^{26}Al measurements, *Quat. Geochronol.*, *3*, 174–195, doi:10.1016/j.quageo.2007.12.001.
- Benson, L. V., J. W. Burdett, M. Kashgarian, S. P. Lund, F. M. Phillips, and R. O. Rye (1996), Climatic and hydrologic oscillations in the Owens Lake basin and adjacent Sierra Nevada, California, *Science*, *274*(5288), 746–748, doi:10.1126/science.274.5288.746.
- Benson, L. V., H. M. May, R. C. Antweiler, T. I. Brinton, M. Kashgarian, J. P. Smoot, and S. P. Lund (1998), Continuous lake-sediment records of glaciation in the Sierra Nevada between 52,600 and 12,500 ^{14}C yr B. P., *Quat. Res.*, *50*(2), 113–127.
- Benson, L., R. Madole, G. Landis, and J. Gosse (2005), New data for late Pleistocene Pinedale alpine glaciation from southwestern Colorado, *Quat. Sci. Rev.*, *24*(1–2), 49–65, doi:10.1016/j.quascirev.2004.07.018.
- Briner, J. P. (2007), Moraine pebbles and boulders yield indistinguishable ^{10}Be ages: A case study from Colorado, USA, *Eos Trans. AGU*, *88*(52), Fall Meet. Suppl., Abstract PP33B–1272.
- Briner, J. P., D. S. Kaufman, W. F. Manley, R. C. Finkel, and M. W. Caffee (2005), Cosmogenic exposure dating of late Pleistocene moraine stabilization in Alaska, *Geol. Soc. Am. Bull.*, *117*(7–8), 1108–1120, doi:10.1130/B25649.1.
- Brugger, K. A. (2005), Equilibrium-line altitudes, snowline gradients, and late-Pleistocene climate in west-central Colorado, *Geol. Soc. Am. Abstr.*, *37*(7), 423.
- Clark, D. H., and A. R. Gillespie (1997), Timing and significance of late-glacial and Holocene cirque glaciation in the Sierra Nevada, California, *Quat. Int.*, *38–39*, 21–38, doi:10.1016/S1040-6182(96)00024-9.
- Clark, P. U., and P. J. Bartlein (1995), Correlation of late Pleistocene glaciation in the western United States with North Atlantic Heinrich events, *Geology*, *23*(6), 483–486, doi:10.1130/0091-7613(1995)023<0483:COLPGI>2.3.CO;2.
- Colgan, P. M., P. R. Bierman, D. M. Mickelson, and M. Caffee (2002), Variation in glacial erosion near the southern margin of the Laurentide ice sheet, south-central Wisconsin, USA: Implications for cosmogenic dating of glacial terraces, *Geol. Soc. Am. Bull.*, *114*(12), 1581–1591, doi:10.1130/0016-7606(2002)114<1581:VIGENT>2.0.CO;2.
- Davis, P. T., P. W. Birkeland, N. Caine, and D. T. Rodbell (1992), New radiocarbon ages from cirques in Colorado Front Range, *Geol. Soc. Am. Abstr. Prog.*, *24*(7), 347.
- Elias, S. A., P. E. Carrara, L. J. Toolin, and A. J. T. Jull (1991), Revised age of deglaciation of Lake Emma based on new radiocarbon and macrofossil analyses, *Quat. Res.*, *36*(3), 307–321.
- Gosse, J. C., E. B. Evenson, J. Klein, B. Lawn, and R. Middleton (1995a), Precise cosmogenic ^{10}Be measurements in western North America: Support for a global Younger Dryas cooling event, *Geology*, *23*(10), 877–880, doi:10.1130/0091-7613(1995)023<0877:PCBMIW>2.3.CO;2.
- Gosse, J. C., J. Klein, E. B. Evenson, B. Lawn, and R. Middleton (1995b), Beryllium-10 dating of the duration and retreat of the last Pinedale glacial sequence, *Science*, *268*(5215), 1329–1333, doi:10.1126/science.268.5215.1329.
- Guido, Z. S., D. J. Ward, and R. S. Anderson (2007), Pacing the post-last glacial maximum demise of the Animas Valley Glacier and the San Juan Mountain ice cap, Colorado, *Geology*, *35*(8), 739–742, doi:10.1130/G23596A.1.
- Hallet, B., L. Hunter, and J. Bogen (1996), Rates of erosion and sediment evacuation by glaciers: A review of field data and their implications, *Global Planet. Change*, *12*(1–4), 213–235, doi:10.1016/0921-8181(95)00021-6.
- Harbor, J. M. (1992), Numerical modeling of the development of U-shaped valleys by glacial erosion, *Geol. Soc. Am. Bull.*, *104*(10), 1364–1375, doi:10.1130/0016-7606(1992)104<1364:NMOTDO>2.3.CO;2.
- Hostetler, S. W., and P. J. Bartlein (1999), Simulation of the potential responses of regional climate and surface processes in western North America to a Canonical Heinrich Event, in *Mechanisms of Global Climate Change at Millennial Time Scales*, *Geophys. Monogr. Ser.*, vol. 112, edited by P. U. Clark, R. S. Webb, and L. D. Keigwin, pp. 313–327, AGU, Washington, D. C.
- Hostetler, S. W., P. U. Clark, P. J. Bartlein, A. C. Mix, and N. J. Piasias (1999), Atmospheric transmission of North Atlantic Heinrich events, *J. Geophys. Res.*, *104*(D4), 3947–3952, doi:10.1029/1998JD200067.
- Kaufman, D. S., S. C. Porter, and A. R. Gillespie (2003), Quaternary alpine glaciation in Alaska, the Pacific Northwest, Sierra Nevada, and Hawaii, *Dev. Quat. Sci.*, *1*, 77–103, doi:10.1016/S1571-0866(03)01005-4.
- Kessler, M. A., R. S. Anderson, and G. Stock (2006), Modeling topographic and climatic control of east-west asymmetry in Sierra Nevada Glacier length during the Last Glacial Maximum, *J. Geophys. Res.*, *111*, F02002, doi:10.1029/2005JF000365.
- Klok, E. J., and J. Oerlemans (2004), Climate reconstructions derived from global glacier length records, *Arct. Antarct. Alp. Res.*, *36*(4), 575–583, doi:10.1657/1523-0430(2004)036[0575:CRDFGG]2.0.CO;2.
- Leonard, E. M. (1984), Late Pleistocene equilibrium-line altitudes and modern snow accumulation patterns, San Juan Mountains, Colorado, U.S., *Arct. Alp. Res.*, *16*(1), 65–76, doi:10.2307/1551173.
- Leopold, M., and D. Dethier (2007), Near surface geophysics and sediment analysis to precisely date the outbreak of glacial Lake Devlin, Front Range Colorado, USA, *Eos Trans. AGU*, *88*(52), Fall Meet. Suppl., Abstract H51E–0809.
- Licciardi, J. M., and K. L. Pierce (2008), Cosmogenic exposure-age chronologies of Pinedale and Bull Lake glaciations in greater Yellowstone and the Teton Range, USA, *Quat. Sci. Rev.*, *27*, 814–831, doi:10.1016/j.quascirev.2007.12.005.
- Licciardi, J. M., P. U. Clark, E. J. Brook, K. L. Pierce, M. D. Kurz, D. Elmore, and P. Sharma (2001), Cosmogenic ^3He and ^{10}Be chronologies of the late Pinedale northern Yellowstone ice cap, Montana, USA, *Geology*, *29*(12), 1095–1098, doi:10.1130/0091-7613(2001)029<1095:CHABCO>2.0.CO;2.
- Licciardi, J. M., P. U. Clark, E. J. Brook, D. Elmore, and P. Sharma (2004), Variable responses of western U.S. glaciers during the last deglaciation, *Geology*, *32*(1), 81–84, doi:10.1130/G19868.1.
- Lifton, N. A., J. W. Bieber, J. M. Clem, M. L. Duldig, P. Evenson, J. E. Humble, and R. Pyle (2005), Addressing solar modulation and long-term uncertainties in scaling secondary cosmic rays for in situ cosmogenic nuclide applications, *Earth Planet. Sci. Lett.*, *239*(1–2), 140–161, doi:10.1016/j.epsl.2005.07.001.
- Loso, M. G., R. S. Anderson, and S. P. Anderson (2004), Post-Little Ice Age record of coarse and fine clastic sedimentation in an Alaskan proglacial lake, *Geology*, *32*(12), 1065–1068, doi:10.1130/G20839.1.
- MacGregor, K. R., R. S. Anderson, S. P. Anderson, and E. D. Waddington (2000), Numerical simulations of glacial-valley longitudinal profile evolution, *Geology*, *28*(11), 1031–1034, doi:10.1130/0091-7613(2000)28<1031:NSOGLP>2.0.CO;2.
- Madole, R. F. (1986), Lake Devlin and Pinedale glacial history, Front Range, Colorado, *Quat. Res.*, *25*(1), 43–54.
- McManus, J. F., R. Francois, J. M. Gherardi, L. D. Keigwin, and S. Brown-Leger (2004), Collapse and rapid resumption of Atlantic meridional circulation linked to deglacial climate changes, *Nature*, *428*(6985), 834–837, doi:10.1038/nature02494.
- Meierding, T. C. (1982), Late Pleistocene glacial equilibrium-line altitudes in the Colorado Front Range; a comparison of methods, *Quat. Res.*, *18*(3), 289–310.
- Menounos, B., and M. A. Reasoner (1997), Evidence for cirque glaciation in the Colorado Front Range during the Younger Dryas chronozone, *Quat. Res.*, *48*(1), 38–47.
- Miller, G. H., J. P. Briner, N. A. Lifton, and R. C. Finkel (2006), Limited ice-sheet erosion and complex exposure histories derived from in situ cosmogenic ^{10}Be , ^{26}Al , and ^{14}C on Baffin Island, Arctic Canada, *Quat. Geochronol.*, *1*, 74–85, doi:10.1016/j.quageo.2006.06.011.
- Munroe, J. S., B. J. C. Laabs, J. D. Shakun, B. S. Singer, D. M. Mickelson, K. A. Refsnider, and M. W. Caffee (2006), Latest Pleistocene advance of alpine glaciers in the southwestern Uinta Mountains, Utah, USA: Evidence for the influence of local moisture sources, *Geology*, *34*(10), 841–844, doi:10.1130/G22681.1.
- Nishiizumi, K., D. Elmore, X. Z. Ma, and J. R. Arnold (1984), ^{10}Be and ^{36}Cl depth profiles in an Apollo 15 drill core, *Earth Planet. Sci. Lett.*, *70*(2), 157–163, doi:10.1016/0012-821X(84)90001-3.
- Nishiizumi, K., E. L. Winterer, C. P. Kohl, J. Klein, R. Middleton, D. Lal, and J. R. Arnold (1989), Cosmic ray production rates of ^{10}Be and ^{26}Al in quartz from glacially polished rocks, *J. Geophys. Res.*, *94*(B12), 17,907–17,915, doi:10.1029/JB094iB12p17907.
- Nishiizumi, K., M. Imamura, M. Caffee, J. Southon, R. Finkel, and J. McAninch (2007), Absolute calibration of ^{10}Be AMS Standards, *Nucl. Instrum. Methods Phys. Res. Sect. B*, *258*, 403–413, doi:10.1016/j.nimb.2007.01.297.
- Oerlemans, J. (1994), Quantifying global warming from the retreat of glaciers, *Science*, *264*(5156), 243–245, doi:10.1126/science.264.5156.243.
- Phillips, F. M., M. G. Zreda, J. C. Gosse, J. Klein, E. B. Evenson, R. D. Hall, O. A. Chadwick, and P. Sharma (1997), Cosmogenic ^{36}Cl and ^{10}Be ages of Quaternary glacial and fluvial deposits of the Wind River Range, Wyoming, *Geol. Soc. Am. Bull.*, *109*(11), 1453–1463, doi:10.1130/0016-7606(1997)109<1453:CCABAO>2.3.CO;2.

- Pierce, K. L. (1979), History and dynamics of glaciation in the northern Yellowstone National Park area, *U.S. Geol. Surv. Prof. Pap.*, 729F, pp. 69–72.
- Pierce, K. L. (2003), Pleistocene glaciations of the Rocky Mountains, *Dev. Quat. Sci.*, 1, 63–76, doi:10.1016/S1571-0866(03)01004-2.
- Porter, S. C. (1975), Glaciation limit in New Zealand's Southern Alps, *Arct. Alp. Res.*, 7(1), 33–37, doi:10.2307/1550096.
- Porter, S. C., K. L. Pierce, and T. D. Hamilton (1983), Late Wisconsin mountain glaciation in the western United States, in *Late-Quaternary Environments of the United States, I. The Late Pleistocene*, edited by H. E. Wright Jr., pp. 71–111, Univ. of Minn. Press, Minneapolis, Minn.
- Refsnider, K. A. (2008), Last glacial maximum climate inferences from cosmogenic dating and glacier modeling of the western Uinta ice field, Uinta Mountains, Utah, *Quat. Res.*, 69, 130–144, doi:10.1016/j.yqres.2007.10.014.
- Reimer, P. J., et al. (2004), IntCal04 terrestrial radiocarbon age calibration, 0–26 cal kyr BP, *Radiocarbon*, 46(3), 1029–1058.
- Riihimaki, C. A., K. R. MacGregor, R. S. Anderson, S. P. Anderson, and M. G. Loso (2005), Sediment evacuation and glacial erosion rates at a small alpine glacier, *J. Geophys. Res.*, 110, F03003, doi:10.1029/2004JF000189.
- Schaefer, J. M., G. H. Denton, D. J. A. Barrell, S. Ivy-Ochs, P. W. Kubik, B. G. Andersen, F. M. Phillips, T. V. Lowell, and C. Schluechter (2006), Near-synchronous interhemispheric termination of the last glacial maximum in mid-latitudes, *Science*, 312(5779), 1510–1513, doi:10.1126/science.1122872.
- Schildgen, T. (2000), Fire and ice: Geomorphic history of Middle Boulder Creek as determined by isotopic dating techniques, CO Front Range, B.S. thesis, Williams Coll., Williamstown, Mass.
- Severinghaus, J. P., and E. J. Brook (1999), Abrupt climate change at the end of the last glacial period inferred from trapped air in polar ice, *Science*, 286(5441), 930–934, doi:10.1126/science.286.5441.930.
- Stone, J. O. (2000), Air pressure and cosmogenic isotope production, *J. Geophys. Res.*, 105(B10), 23,753–23,759, doi:10.1029/2000JB900181.
- Stuiver, M., and P. J. Reimer (1993), Extended ¹⁴C data base and revised CALIB 3.0 ¹⁴C age calibration program, *Radiocarbon*, 35(1), 215–230.
- Toney, J. L., and R. S. Anderson (2006), A postglacial palaeoecological record from the San Juan Mountains of Colorado USA: Fire, climate and vegetation history, *Holocene*, 16(4), 505–517, doi:10.1191/0959683606hl946rp.

R. S. Anderson, Z. S. Guido, and D. J. Ward, Department of Geological Sciences and Institute for Arctic and Alpine Research, University of Colorado, Boulder, CO 80309, USA. (dylan.ward@colorado.edu)
 J. P. Briner, Department of Geology, State University of New York at Buffalo, Buffalo, NY 14260, USA.